AD-E430677

(12) LEVEL III

AD

AD A104382

TECHNICAL REPORT ARBRL-TR-02345

DEVELOPMENT OF INVERSE RAMAN SPECTROSCOPY FOR PROBING RAPIDLY DECOMPOSING EXPLOSIVES AND PROPELLANTS

David R. Crosley
Michael A. Schroeder

July 1981

US ARMY ARMAMENT RESEARCH AND DEVELOPMENT COMMAND
BALLISTIC RESEARCH LABORATORY
ABERDEEN PROVING GROUND, MARYLAND

Destroy this report when it is no longer needed.
Do not return it to the originator.

Secondary distribution of this report by originating or sponsoring activity is prohibited.

Additional copies of this report may be obtained from the National Technical Information Service, U.S. Department of Commerce, Springfield, Virginia 22161.

The findings in this report are not to be construed as an official Department of the Army position, unless so designated by other authorized documents.

The use of trade names or manufacturers' names in this report does not constitute indorsement of any commercial product.

UNCLASSIFIED
SECURITY CLASSIFICATION OF THIS PAGE (When Data Entered)

REPORT DOCUMENTATION PAGE	READ INSTRUCTIONS BEFORE COMPLETING FORM
1. REPORT NUMBER: TECHNICAL REPORT ARBRL-TR-02345	2. GOVT ACCESSION NO.: AD-A104382
	3. RECIPIENT'S CATALOG NUMBER
4. TITLE (and Subtitle): DEVELOPMENT OF INVERSE RAMAN SPECTROSCOPY FOR PROBING RAPIDLY DECOMPOSING EXPLOSIVES AND PROPELLANTS	5. TYPE OF REPORT & PERIOD COVERED: BRL Technical Report
	6. PERFORMING ORG. REPORT NUMBER
7. AUTHOR(s): David R. Crosley* Michael A. Schroeder	8. CONTRACT OR GRANT NUMBER(s)
9. PERFORMING ORGANIZATION NAME AND ADDRESS: U.S. Army Ballistic Research Laboratory ATTN: DRDAR-BLI Aberdeen Proving Ground, MD 21005	10. PROGRAM ELEMENT, PROJECT, TASK AREA & WORK UNIT NUMBERS: 1L161102AH43
11. CONTROLLING OFFICE NAME AND ADDRESS: U.S. Army Armament Research & Development Command U.S. Army Ballistic Research Laboratory ATTN: DRDAR-BL Aberdeen Proving Ground, MD 21005	12. REPORT DATE: JULY 1981 13. NUMBER OF PAGES: 76
14. MONITORING AGENCY NAME & ADDRESS(if different from Controlling Office)	15. SECURITY CLASS. (of this report): UNCLASSIFIED 15a. DECLASSIFICATION/DOWNGRADING SCHEDULE

16. DISTRIBUTION STATEMENT (of this Report)

Approved for public release, distribution unlimited

17. DISTRIBUTION STATEMENT (of the abstract entered in Block 20, if different from Report)

18. SUPPLEMENTARY NOTES

*Present address: Molecular Physics Laboratory, SRI International, Menlo Park CA 94025

19. KEY WORDS (Continue on reverse side if necessary and identify by block number)

Inverse Raman spectroscopy
Coherent Antistokes Raman Spectroscopy
TNT
Thermal Decomposition
Laser diagnostics

20. ABSTRACT (Continue on reverse side if necessary and identify by block number) (jmk)

The techniques of inverse Raman spectroscopy and coherent anti-stokes Raman spectroscopy are considered for the purpose of development of rapid (single-shot) broad band detection of species in rapidly (explosively) decomposing materials. Experiments using inverse Raman spectroscopy with pulsed ruby laser, broad-band dye, 1-m spectrometer and optical multichannel analyzer are described. Results on benzaldehyde (neat and in mixtures with toluene) yield information on the quantitative limits of inverse Raman detection.

DD FORM 1 JAN 73 1473 EDITION OF 1 NOV 65 IS OBSOLETE

UNCLASSIFIED

SECURITY CLASSIFICATION OF THIS PAGE (When Data Entered)

TABLE OF CONTENTS

TABLE OF CONTENTS (Cont'd)

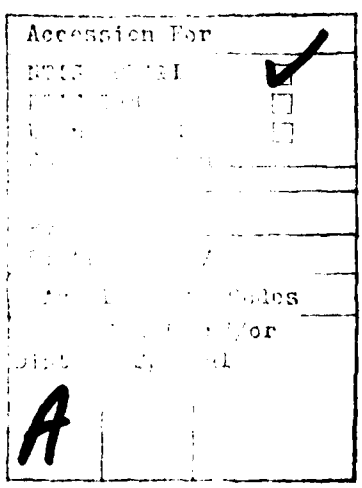

LIST OF ILLUSTRATIONS

LIST OF ILLUSTRATIONS (Cont'd)

LIST OF TABLES

I. INTRODUCTION

The motivation behind this project is the need to develop a rapid, remote spectroscopic probe of a condensed phase energetic material. The envisioned end application is species diagnostics carried out on a liquid - e.g., TNT or a liquid propellant - undergoing shock-induced decomposition within a blast chamber.

Of several candidate laser-based probe methods, one - inverse Raman spectroscopy, hereinafter referred to as IRS - has been under investigation at the Ballistic Research Laboratory. This project was begun by Dr. William VonHolle, whose findings are detailed in a memorandum report[1]. VonHolle carried out experiments on static samples, establishing the quantitative nature of the technique on mixtures of benzene and nitromethane, and performing a survey probe of a candidate liquid propellant which had been refluxed until explosive decomposition occurred. VonHolle concluded[1] that a continuation of the development of IRS, toward the application of probing of a shocked liquid, was warranted.

This report describes our further experiments using the apparatus assembled and tested by VonHolle. The systems probed have been static samples of stable liquids, and the focus has been the establishment of limits of sensitivity, reproducibility and accuracy so as to (i) obtain a clearer assessment of the feasibility of IRS for the probing of an actual shocked liquid, and (ii) provide the necessary criteria for proper experiment design for future applications. In addition, a major improvement in the apparatus has been incorporated - the replacement of the photographic detection method used by VonHolle by an optical multichannel analyzer (OMA), which provides broad-band photoelectric detection capability.

The report is divided into several parts. The next section considers the necessary requirements of a probe system, and a qualitative description of several possible candidate methods. This is followed by a more quantitative explication of IRS, together with our experimental results. We conclude with an outline of future work. There we consider in particular the decomposition of TNT, which has been chosen as a prototype system for study; this choice is governed by a need to consider an actual species for assessing feasibility, combined with a promise of obtaining immediately useful results. In addition, we suggest a direct comparison of IRS and Coherent Anti-stokes Raman Scattering (CARS) for the purpose of rapid, remote probing, and a ramification of IRS (fixed-frequency probe laser) for determining unknown Raman spectra of pertinent compounds.

---

[1] *W. VonHolle, "The Application of Inverse Raman Spectroscopy to Chemical Decomposition in Energetic Systems", BRL Memorandum Report No. 2607, March 1976.* (AD #B010506L)

II. PROBE METHODS

A. Requirements

The information sought from the ultimate measurement system consists of species concentrations in a condensed phase, so as to elucidate the reactive mechanism of the rapidly changing energetic material under study. To provide this, several requirements on the probe system - dictated by the nature of the detonative experiment - must be fulfilled. In general, these are: fast time resolution, the capability for remotely probing, and an extensive coverage of many known or suspected species.

In addition, there exists the important question of requisite sensitivity. This should be addressed with reference to the particular system to be probed. A primary objective of the current project has been the establishment of sensitivity parameters under realistic operating conditions, and we later specifically examine the TNT system in this connection.

Another generally desirable requirement, of course, of any experimental method is ease of use. Let it suffice here to note that, at the present time, any of the possible laser-based techniques which fulfill the general criteria listed above all utilize state-of-the-art technology and still-developing methodology. Consequently, the application of any of them to a real system is by no means routine, but is in itself a full research project requiring an investigator intimately acquainted with the apparatus.

1. Time Resolution. In order to obtain a meaningful species profile during a detonation process, it is necessary that the sampling time be short enough that there occurs no averaging over any appreciable chemical reaction. This is accomplished experimentally by using a single shot from a laser of short pulse length. The techniques considered below incorporate Q-switched ruby or neodymium lasers, or perhaps a nitrogen-pumped dye laser. Typical pulse lengths of each of these is of the order of 10 nsec, which thus represents the available sampling time. This is shorter than solution reaction times for all but the fastest ion-ion reactions under diffusion control. While picosecond laser techniques are now in operation at several laboratories, the delicacy of the experimental apparatus involved precludes their consideration for the intended purpose at the present time.

It should be noted that, while the sampling times of 10 nsec are sufficiently short, only one shot per detonation can be made with currently available technology. The highest repetition rate of the lasers listed above is 60 Hz, and more typically it is < 0.1 Hz. Thus the experimental data will furnish a single 'snapshot' of the detonative process, not a 'movie'.

2. Remote probing. In order to study a detonative process, it is desirable to place the sample in some container which is in turn kept within a blast chamber well shielded and removed from the measurement apparatus and operators. This precludes the use of established linear techniques such as spontaneous Raman scattering (SRS) or laser-excited fluorescence (LEF). In each the sample is irradiated with a single laser. Light scattered at Raman shifted frequencies (SRS) or emitted at frequencies characteristic of the excited electronic state (LEF) is focused onto some detector. However, the light is scattered or reemitted into all 4π steradians; the size of the blast chamber, practical limits on the diameter of expendable lenses, and apertures of necessary windows all limit the collection solid angle so that little signal can be obtained from a remotely situated sample*.

Applicable methods, rather, utilize laser light itself as the mode of detection. All of the appropriate schemes involve irradiation of the sample with two lasers. As will be described in more detail below, one detects absorption or polarization rotation of one of the lasers, or a third laser beam generated within the sample. This permits the lasers and the detection apparatus to be placed far from the detonating sample with no attendant loss of signal. An important disadvantage, on the other hand, arises from the need to focus both laser beams simultaneously upon a small sample located some distance away. Thermal drift, vibration, etc., make this a non-trivial problem when considering undertaking an actual experiment.

3. Broad-band detection. Each of the techniques considered produce resonant signals at Raman-shifted frequencies. With only a single shot per detonation possible, spectral information at only one frequency is useless. Instead, one wishes to obtain a broad spectral coverage. This can be done by using as one of the two lasers a dye laser operated broad-band, that is, lasing over the entire gain profile of the dye with no added tuning elements. Typical useful dyes each have ranges of coverage over $\sim$ 150 cm^{-1} with a center frequency dictated by the dye itself, the solvent and the concentration used. Whether the choice of range and center frequency are adequate can be ascertained only by reference to a specific molecular system.

One could extend the wavelength coverage somewhat by using a mixture of dyes. Two (or more) separate regions could be probed by splitting the pump beam and using it to simultaneously pump more than one broad-band dye laser. However, in our experiments we are also limited by the finite size of the OMA photodiode array; in conjunction with a 1-m monochromator its coverage ($\sim$ 250 cm^{-1}) closely matches the output profile of a single dye. Operation over a larger range would require a

---

*Other considerations also rule out these methods. SRS is a very weak effect, and LEF likely suffers from severe interference problems when applied to condensed-phase mixtures of the type of compounds considered here.

monochromator of smaller dispersion, and concomitant decrease in resolution; alternatively, but expensively, one could use two (or more) monochromators and OMAs.

4. Sensitivity limits. While the necessary sensitivity (and accuracy) must be considered in the context of a specified experiment, a general guideline may be given. The three most attractive methods all suffer from some limits on their sensitivity for condensed phase systems. The primary difficulty with IRS is that inherent in any absorption experiment, *viz.*, noise in the probe laser source which prevents detection of absorption below 1-2%. In CARS, non-resonant background signals are of the order of 0.1% of the resonant peaks. In RIKES*, leakage through polarizing filters and birefringence of optical components sets the limit. As a result, selection of strong Raman lines for detection should provide detectability down to mole fractions of the order of 0.01, for a single-shot experiment using any of these techniques.

B. The Family of Coherent Raman Techniques

When a medium is irradiated by an intense enough electric field- as from a high power laser - the non-linear parts of the molecular polarizability produce significant effects[2]. Frequency doubling and optical parametric frequency generation in crystals are examples of effects of the second-order susceptibility $\chi^{(2)}$ which have found widespread application and standard commercial availability**. The third-order susceptibility $\chi^{(3)}$ gives rise to a number of three-wave and four-wave mixing processes. In general, and provided the pertinent selection rules are met, resonances in $\chi^{(3)}$ occur when some difference of the frequencies involved is equal to a Raman frequency in the molecule involved. A variety of these so-called coherent Raman techniques*** has been discovered and, to varying degrees, developed within the past decade. Those suitable for fulfilling the requirements outlined above are IRS, CARS, and Raman-induced Kerr effect spectroscopy (RIKES). Closely related to the IRS is stimulated Raman gain (SRG); another method, coherent stokes Raman spectroscopy (CSRS) is the stokes-shifted counterpart of CARS. In addition there is a series of more complex processes; Hyper-Raman effect, "submarine", "asterisk", "horses", and "boxcars", each having a different dependence on $\chi^{(3)}$. Reference 3 contains a comparison of all the techniques

---

[2] *N. Bloembergen, Non-linear Optics, Benjamin, New York, 1965.*

* *See below.*

** *For Liquids and gases, $\chi^{(2)}$ is zero by symmetry considerations and $\chi^{(3)}$ is the first non-linear term of importance.*

*** *The Russian literature uses the term, 'active Raman spectroscopy'.*

(except the hyper-Raman effect[4], "horses"[4], and "boxcars"[5], in terms of $\chi^{(3)}$.

1. A simple picture. A physical description of some of these processes is described in Figure 1. It should be emphasized that all of these processes actually involve the simultaneous mixing of several light waves, although a conceptual description is facilitated by viewing sequential 'absorptions' and 'emissions' to virtual levels.

SRS is shown in Figure 1a. A laser at frequency ω_1 excites the molecule which scatters light at the stokes frequency $\omega_2 = \omega_1 - \omega_R$, where ω_R is some Raman-active vibrational frequency* in the sample. If there exists a sufficient number of molecules in the excited vibrational level, i.e., if the temperature is hot enough, antistokes radiation ($\omega_2 = \omega_1 + \omega_R$) is scattered (Figure 1b).

In Figure 1c, SRG is shown. If the pumping laser at ω_1 is intense enough, the medium irradiated can exhibit gain at $\omega_2 = \omega_1 - \omega_R$. A coherent beam, unidirectional and more or less** along the path of the pump laser, is emitted by the sample.

A strong pump laser at ω_1 can also induce downward transitions from the virtual state (Figure 1d), provided there exist photons available at $\omega_2 = \omega_1 + \omega_R$ such that the molecules can 'populate' the virtual state. This is the basis of IRS. The photons at ω_2 are usually furnished by a broadband dye laser pumped simultaneously by frequency-doubled radiation from the laser at ω_1. Absorption of the dye beam occurs at all frequencies ω_2 which are separated from ω_1 by a Raman frequency of the sample. The unidirectional dye laser beam is then focussed onto the slit of a monochromator, which disperses it so as to measure the frequencies ω_2 at which absorption has occurred. The effective absorption coefficient depends on the power of the laser at ω_1 and the two lasers must of course overlap spatially as well as temporally.

---

[3] *W. M. Tolles, G. L. Eesley and M. D. Levenson, "Heterodyne Detection of Coherent Signals", S.P.I.E. Conference, San Diego, Cal., August 1977.*

[4] *A. C. Eckbreth, P. A. Bonczyk and J. F. Verdieck, "Laser Raman and Fluorescence Techniques for Practical Combustion Diagnostics", Appl. Spec. Rev. 12, 15-164 (1978).*

[5] *A. C. Eckbreth, "BOXCARS: Crossed-Beam Phase-Matched CARS Generation in Gases", Appl. Phys. Lett., to be published.*

* *Rotational and electronic Raman effects also exist but are not suitable for the current purpose.*

** *Depending on the variation of the refractive index of the medium with frequency.*

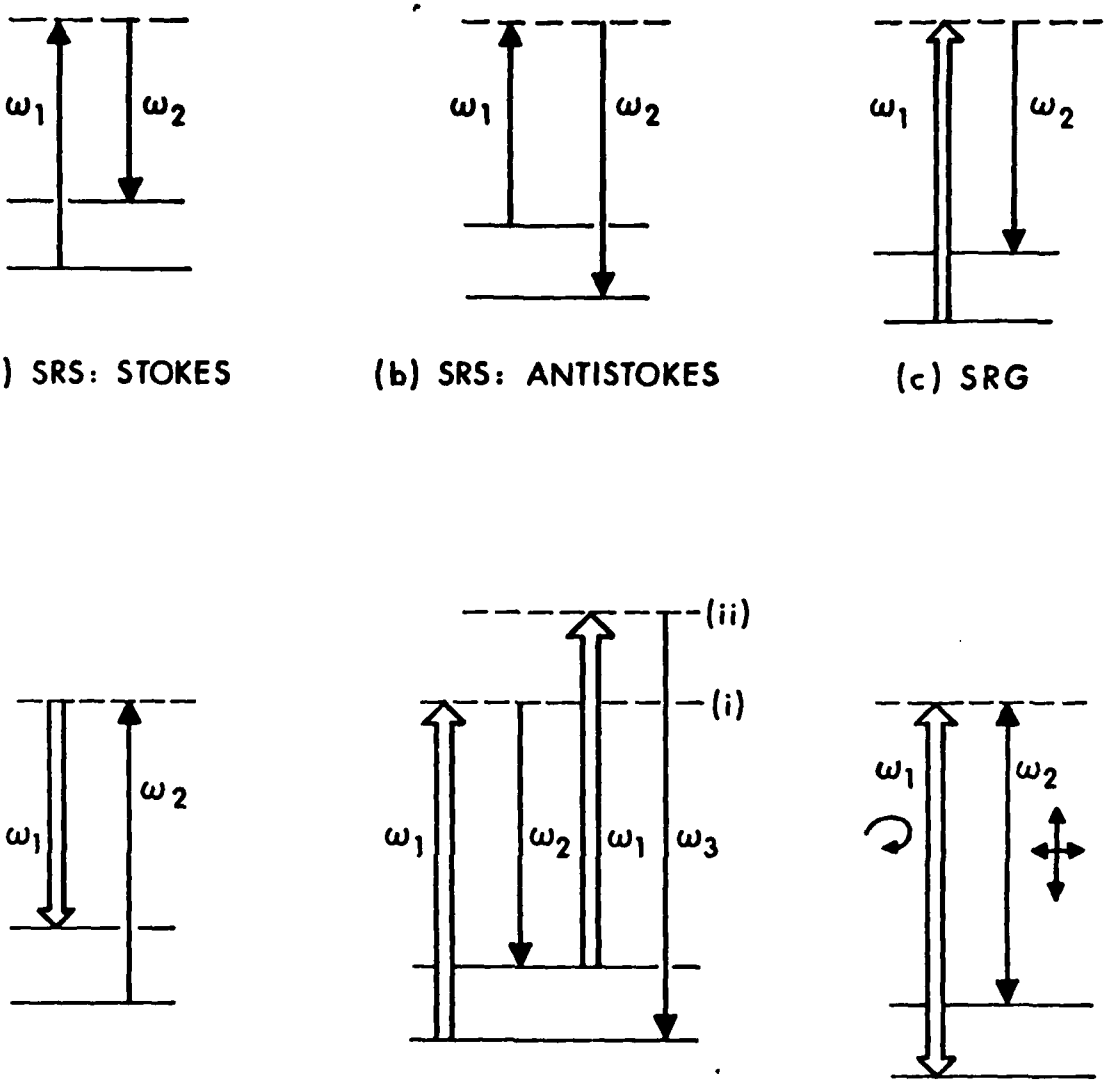

Figure 1. Transitions involved in different Raman processes. Solid lines indicate real levels, while dashed lines denote virtual states. (a) spontaneous Raman scattering in Stokes region; (b) spontaneous Raman scattering in anti-Stokes region; (c) stimulated Raman gain; (d) inverse Raman spectroscopy; (e) coherent anti-Stokes Raman spectroscopy; (f) Raman-induced Kerr effect spectroscopy. For the coherent Raman techniques (c) - (f), the stronger (pump) laser is designated by a broad, open arrow and the probe laser is shown as a thin arrow. In RIKES, (f), the pump laser is circularly polarized, and the probe laser is linearly polarized. Signal at ω_2, polarized perpendicularly to the incident beam, is detected.

CARS (Figure 1e) is a four-wave mixing process in which two frequencies are the same. The higher power laser at ω_1 elevates molecules to a virtual state i, from which they are stimulated downward to the excited vibrational level by the second laser at ω_2. From here, the laser at ω_1 pumps them to a second virtual state ii, from which a coherent beam at $\omega_3 = 2\omega_1 - \omega_2$ is generated. Although some light at ω_3 is generated for any combination of ω_1 and ω_2, strong resonances occur when $\omega_2 = \omega_1 - \omega_R$ (as indicated in the figure). The use of a broadband dye laser at ω_2 generates several coherent beams at different values of ω_3 corresponding to different Raman frequencies. As in IRS, a monochromator separates the wavelengths to provide the data.

In RIKES, Figure 1f, a strong circularly polarized pump beam at ω_1 induces a birefringence in the sample. A probe beam at ω_2 is linearly polarized in the vertical direction prior to entering the sample. A horizontal polarizer following the sample passes no radiation at ω_2 except for some small amount which has been rotated due to the birefringence induced by the pump beam at ω_1. Again, strong resonances occur when $\omega_2 = \omega_1 - \omega_R$, and again a broadband laser beam furnishing ω_2 may be dispersed to measure those frequencies at which there occurs transmission between the crossed polarizers.

2. Some ramifications. A number of modifications of the coherent Raman effects have been proposed and/or tried in order to enhance sensitivity or decrease noise.

When the pump laser at ω_1 in Figure 1 is at such a frequency that the virtual state approaches an actual electronic state, resonant enhancement of any Raman signal occurs. This has been demonstrated for IRS[6] as well as the other methods. However, the ability to exploit the resonant enhancement requires a match between electronic absorption frequencies and available lasers, not usually possible for multi-species work.

Absorption of any laser radiation can be dramatically increased by placement of the sample inside the laser cavity, where absorption spoils the gain and produces non-linear effects. Again, this is nominally suitable for IRS on a static sample[7]; however our experience suggests that it would be exceedingly difficult to maintain proper cavity alignment through a remotely situated sample. In addition, windows and shock-generated turbulence may also cause losses.

---

[6] *S. H. Lin, E. S. Reid and C. J. Tredwell, "The Resonance Inverse Raman Effect", Chem. Phys. Lett. 29, 389-392 (1974).*

[7] *W. Wernecke, J. Klein, A. Lau, K. Lenz, and G. Hunsalz, "Investigation of Inverse Raman Spectroscopy using the Method of Intracavity Spectroscopy", Opt. Comm. 11, 159-163 (1974).*

Optical heterodyning[8] involves mixing of the signal beam from the sample with part of the probe beam split off prior to entering the sample. Published reports[3,6] have considered so far only application to RIKES using a relatively quiescent probe laser. Results of a preliminary study[9] indicate that optical heterodyning does not so far improve signal-to-noise in a single-shot RIKES experiment due to other sources of limiting noise.

3. Comparing the techniques. The three methods, IRS, CARS and RIKES, appear to be the suitable current candidates as remote, broadband probes of rapidly evolving energetic materials.

Each may be operated using as the pump laser a pulsed source in the 10 nsec region. Each involves the detection of a coherent beam and is thus suitable for remote work.

The broadband nature of detection has been demonstrated for IRS[1]; the first RIKES experiment was performed in this manner[10]. Broadband CARS experiments have been performed in the gas phase[11], in the way described above. Now because of the three-wave mixing involved in CARS, it is necessary to match wavevectors (conserve momentum) as well as energy. Since $|k| \approx \frac{\omega}{\pi c}$, a medium in which n varies rapidly with ω will prevent momentum conservation over a broad frequency regime. This is not a problem with gases, but could be so for liquids. To date, no broadband CARS experiments on liquids have been reported. Instead, a narrow band tunable laser is used at ω_2. However, in one early experiment a tuning range of ~ 150 cm^{-1} was covered[12] with no need to adjust phase-matching angles over this region[13]. Consequently it appears that broadband CARS should be viable for liquids over the untuned gain profile of a single dye.

---

[8] *G. L. Eesley, M. D. Levenson, and W. M. Tolles, "Optically Heterodyned Coherent Raman Spectroscopy", J. Quant. Elec., to be published.*

[9] *W. VonHolle, private communication, May 1978.*

[10] *D. Heiman, R. W. Hellwarth, M. D. Levenson and G. Martin, "Raman-Induced Kerr Effect", Phys. Rev. Lett. 36, 189-192 (1976).*

[11] *W. B. Roh, P. W. Schreiber and J. P. E. Taran, "Single-pulse Coherent Anti-Stokes Raman Spectroscopy", Appl. Phys. Lett. 29, 174-176 (1976).*

[12] *R. F. Begley, A. B. Harvey, R. L. Byer and B. S. Hudson, "Raman Spectroscopy with Intense, Coherent Anti-Stokes Beams", J. Chem. Phys. 61, 2466-2467 (1974).*

[13] *A. B. Harvey, private communication, May 1978.*

To our knowledge, there are only two current investigations of these methods aimed at the remote, rapid, broadband sampling of a condensed phase. There is of course the present study, begun by VonHolle and continued by ourselves. In addition to the development of IRS, we feel it is desirable to carry out in the future a comparison with single-shot CARS. VonHolle, now at Lawrence Livermore Laboratory, is continuing work on IRS of energetic materials, and has recently succeeded at performing a single-shot optically-heterodyned RIKES measurement[9].

It should be emphasized that at the present time there is no reason to consider any technique necessarily superior, nor to even project that any one will ultimately be best for all investigations. Through our and VonHolle's further characterization of IRS, his work on RIKES, and our projected trial of CARS, there will hopefully grow a large enough body of data to permit proper experimental design and to provide useful concentrations.

III. THE INVERSE RAMAN ABSORPTION COEFFICIENT

A. Phenomenological Derivation

We present a brief phenomenological derivation of the absorption coefficient pertinent to IRS, in a form suitable for the insertion of previously measured or estimable parameters for the purpose of assessing signal levels.

In a conventional SRS experiment (Figure 1a), the total intensity in photons sec^{-1} - over the whole Raman line - spontaneously scattered into all 4π steradians and over the differential path length dx, is given by

$$dI_s = 4\pi N\left(\frac{d\sigma}{d\Omega}\right) I_L \, dx \, . \qquad (1)$$

Here, N is the molecular sample density (cm^{-3}), $\frac{d\sigma}{d\Omega}$ is the differential Raman scattering cross section ($cm^2\ sr^{-1}$), and I_L is the intensity (photons sec^{-1}) incident upon the sample. (Normally, in SRS, there is no appreciable attenuation of the beam along the sample length, and Eq. (1) is usually presented in the integrated form $I_s = 4\pi N\ell\left(\frac{d\sigma}{d\Omega}\right) I_L$ where ℓ is the total path length over which the observation is made).

Consider the case in which there exists sufficient photon density at I_s so that stimulated scattering is important as well as spontaneous scattering (as in SRG, Figure 1c, and IRS, Figure 1d). Then the scattering probability W is a sum of two terms, fully analogous to the situation found for stimulated and spontaneous emission from a real state. These

two terms are usually written[14]

$$W \propto \frac{8\pi h \nu_s^3 n_s^3}{c^3} + \rho(\nu_s) \quad , \tag{2}$$

where ν_s is the frequency (Hz) and n_s is the refractive index at the Stokes frequency. $\rho(\nu_s)$ is the spectral energy density at this frequency, in units of erg cm^{-3} Hz^{-1}. It is convenient to integrate Eq. (2) over frequency, so as to obtain the total energy within the line. Then

$$\int W d\nu \propto \frac{8\pi h \nu_s^3 n_s^3 \Delta\nu}{c^3} + \int \rho(\nu_s) d\nu \quad , \tag{3}$$

where $\Delta\nu$ is the linewidth of the (spontaneous) Raman transition. $\int \rho(\nu_s) d\nu$ represents the total energy density (erg cm^{-3}), available in the radiation field, at the frequency ν_s (in the inverse Raman experiment, this energy is provided by the pump laser).

In Eq. (3), the first term on the right-hand side represents the total energy within the spontaneous Raman line, thereby serving to define $\Delta\nu$. For example, were the Raman lineshape triangular, $\Delta\nu$ would simply be the full width at half maximum. For a Lorentzian lineshape, $\Delta\nu$ would be $\frac{\pi}{2}$ times the full width at half maximum.

Now Eq. (1) describes only the spontaneous scattering. For the case such as IRS in which the stimulated emission totally dominates, $\int \rho(\nu_s) d\nu >> \frac{8\pi h \nu_s^3 n_s^3 \Delta\nu}{c^3}$. Then the expression for dI_s in Eq. (1) becomes greater by the ratio of these two terms, and we have

$$dI_s = \frac{N\left(\frac{d\sigma}{d\Omega}\right) I_L c^3 \int \rho(\nu_s) d\nu \, dx}{2h\nu_s^3 n_s^3 \Delta\nu} \quad . \tag{4}$$

But, by conservation of energy, the number of Stokes photons created at ν_s within the medium must equal the number of photons removed from the beam at the frequency ν_L.

---

[14] *M. A. Koningstein, Introduction to the Theory of the Raman Effect, D. Reidel, Dordrecht, Holland, 1972, p. 142-144.*

$$dI_L = - dI_s = - \frac{N(\frac{d\sigma}{d\Omega})\ I_L c^3 \int\rho(\nu_s)\ d\nu\ dx}{2h\nu_s^3\ n_s^3\ \Delta\nu} \quad . \tag{5}$$

Under conditions in which the energy density $\int\rho(\nu_s)d\nu$ does not vary* with x, Eq. (5) may be readily integrated over a path length ℓ:

$$I_L(\ell) = I_L(0)\ \exp\ (-\ \alpha\ell) \tag{6}$$

where we define α (with units of cm^{-1}) as the inverse Raman absorption coefficient

$$\alpha = \frac{N(\frac{d\sigma}{d\Omega})\ c^3 \int\rho(\nu_s)d\nu}{2h\nu_s^3\ n_s^3\ \Delta\nu} \quad , \tag{7}$$

It is convenient to express the energy density in terms of the power density $P(\nu_s)$, in watt cm^{-2}. For a laser of pulse length τ, cross-sectional beam area A and energy per pulse $E(\nu_s)$,

$$\int\rho(\nu_s)d\nu = \frac{E(\nu_s)}{V} = \frac{E(\nu_s)n_s}{Ac\tau} = \frac{10^7 P(\nu_s)n_s}{c} \quad . \tag{8}$$

V is the volume occupied by the pulse, and is the product of A and the effective pulse length $c\tau/n_s$. We rewrite Eq. (7) using Eq. (8), and also converting all frequencies ν (Hz) to vacuum cm^{-1}, denoted by $\omega = \nu/c$. Then

$$\alpha = \frac{10^7 N(\frac{d\sigma}{d\Omega})\ P(\omega_s)}{2hc^2\omega_s^3\ n_s^2\ \Delta\omega} \tag{9}$$

which forms the desired result of this section.

*We later consider such a variation.

B. Other Expressions

Yeung[15] also presents a derivation of α which can be obtained from his Eq. (7) for stimulated Raman gain. We contend that Yeung does not properly introduce the Raman linewidth $\Delta\nu$; he considers it as the bandwidth of the energy density available at ν_s, but this is not the case when that energy density is supplied by a pumping laser as in IRS. Rather, the integration expressed in our Eq. (3) maintains consistency and generality for any source of $\rho(\nu_s)$.

Nonetheless Yeung's result agrees with our own. In addition, Yeung presents a critique of other expressions for α (or its SRG counterpart), pointing out inconsistencies and some lack of care in defining units.

In particular, we note that the expression for the stimulated Raman gain coefficient g in Eq. (2) of Grun, McQuillan and Stoicheff[16] considers a Lorentzian linewidth so that their $\pi\Delta\nu/2$ is equivalent to our $\Delta\nu$. Nonetheless α of Eq. (9) is a factor of 2 smaller than the equivalent of their formula. This is uncomfortable in view of the excellent agreement they obtain between g calculated from that equation and g measured in experiments on liquid N_2 and O_2. We do note that they quote estimated errors of the order of 50%. We cannot reconcile our expression with that of Werncke, et al.,[7] for which we have also had difficulty in attaining dimensional consistency.

We have chosen to express α in terms of the differential Raman scattering cross section, a microscopic (i.e., per molecule) quantity. This will facilitate estimations of α for different compounds using relative intensities from standard collections of spontaneous Raman spectra[17]. However, much of the current coherent Raman literature expresses transition probabilities in terms of the third-order susceptibility $\chi^{(3)}$, a macroscopic quantity. The resonant part of $\chi^{(3)}$ is related to $d\sigma/d\Omega$ by[18]

---

[15] *E. S. Yeung, "Inverse Raman Effect: A Quantitative Spectroscopic Technique", J. Mol. Spec. 53, 379-392 (1974).*

[16] *J. B. Grun, A. K. McQuillan and B. P. Stoicheff. "Intensity and Gain Measurements on the Stimulated Emission in Liquid O_2 and N_2", Phys. Rev. 180, 61-68 (1969).*

[17] *B. Schrader and W. Meier, ed., Raman/IR Atlas of Organic Compounds. Verlag Chemie, Weinheim, 1974.*

[18] *W. M. Tolles, J. W. Nibler J. R. McDonald, and A. B. Harvey, "A Review of the Theory and Application of Coherent Anti-Stokes Raman Spectroscopy (CARS)", Appl. Spect. 31, 253-271 (1977).*

$$3\chi^{(3)} = \frac{N\frac{d\sigma}{d\Omega}}{8\pi^3 hc\omega_s^4} \cdot \frac{1}{2\delta - i\Delta\omega} \quad . \tag{10}$$

$\chi^{(3)}$ is both complex and frequency dependent; δ represents the amount of detuning from resonance (all frequencies here are expressed in cm^{-1}). At resonance,

$$3|\chi^{(3)}| = \frac{N\frac{d\sigma}{d\Omega}}{8\pi^3 hc\omega_s^4 \Delta\omega} \quad . \tag{11}$$

The Raman scattering cross section can also be written in terms of molecular parameters. The relationship is[16]

$$\frac{d\sigma}{d\Omega} = \frac{hc\omega_s^4}{2\mu\omega_R} \left(\bar{\alpha}'^2 + \frac{7}{45}\beta'^2\right) \tag{12}$$

where μ is the reduced mass and ω_R the frequency (cm^{-1}) of the vibration in question. $\bar{\alpha}'$ and β' are the isotropic and anisotropic parts, respectively, of the derivative of the polarizability with respect to the appropriate internuclear coordinate, and evaluated at the equilibrium position. $\bar{\alpha}$ is known as the mean polarizability and β is the anisotropy.

C. Degree of Polarization of Raman Lines

Classical electromagnetic theory shows that, for linearly polarized light incident upon an isotropic (spherically symmetric) system, the scattered light (Rayleigh or Raman) will have its polarization direction parallel to that of the incident light. This is because the dipole induced by the incoming electric field is parallel to that field, and must also radiate a field vector parallel to itself.

A molecular system, on the other hand, has three principal axes, along each of which the polarizabilities are not necessarily equal*. In a macroscopic sample the molecules will be randomly oriented with respect to the incident light electric vector. Consequently a moment induced by this field will not in general be parallel to the electric vector, and the scattered radiation will contain components polarized perpendicularly to the incident electric vector.

---

*If equal, the molecular polarizability is spherically symmetric, e.g., in CH_4.

The polarizability tensor $\underline{\alpha}$ can be written in terms $\bar{\alpha}$ and β, which are invariants $\underline{\alpha}$. A consideration of the relationship[19] of the cartesian components of $\underline{\alpha}$ to $\bar{\alpha}$ and β leads to a direct identification with experimental measurements. The degree of depolarization, or depolarization ratio ρ, is defined in terms of the intensity of scattered radiation whose polarization is perpendicular to the plane of polarization of the incident light, divided by the intensity of light polarized parallel to that plane. (See Figure 2).

If the incident light is unpolarized,

$$\rho_u = \frac{I_\perp}{I_{//}} = \frac{6\beta^2}{45\bar{\alpha}^2 + 7\beta^2} \quad , \tag{13a}$$

while if it is polarized (at 90° to the direction of observation),

$$\rho_p = \frac{I_\perp}{I_{//}} = \frac{3\beta^2}{45\bar{\alpha}^2 + 4\beta^2} \tag{13b}$$

the smallest possible value of ρ is zero, which occurs when there is no anisotropy and corresponds to classical scattering from a spherical system. The largest values ρ can attain are 6/7 for unpolarized light and 3/4 for linearly polarized light. It can be shown[20] that this occurs only for non-totally symmetric vibrations; a vibration showing ρ less than these values must be totally symmetric.

The inverse Raman effect depends on the coupling of an induced dipole moment with the electric field vectors of two light waves. One could argue classically and qualitatively that a totally isotropic polarizability ($\rho=\beta=0$) would thus couple the electric fields only if they were polarized parallel to one another. However, consider a vibration having ρ nearer its maximum attainable value. Here, a dipole moment induced by one electric field vector will have appreciable components in a perpendicular direction. Hence, for such a so-called depolarized Raman line, there should be appreciable inverse Raman absorption regardless of the relative polarizations of the lasers at ω_s and ω_L.

This aspect has previously been experimentally investigated using intracavity inverse Raman absorption[7]. In the spectrum of toluene,

---

[19] *D. Steele, Theory of Vibrational Spectroscopy, Saunders, Philadelphia, 1971, p. 166ff.*

[20] *G. Herzberg, Molecular Spectra and Molecular Structure. II. Infrared and Raman Spectra of Polyatomic Molecules, D. Van Nostrand, Princeton, 1945.*

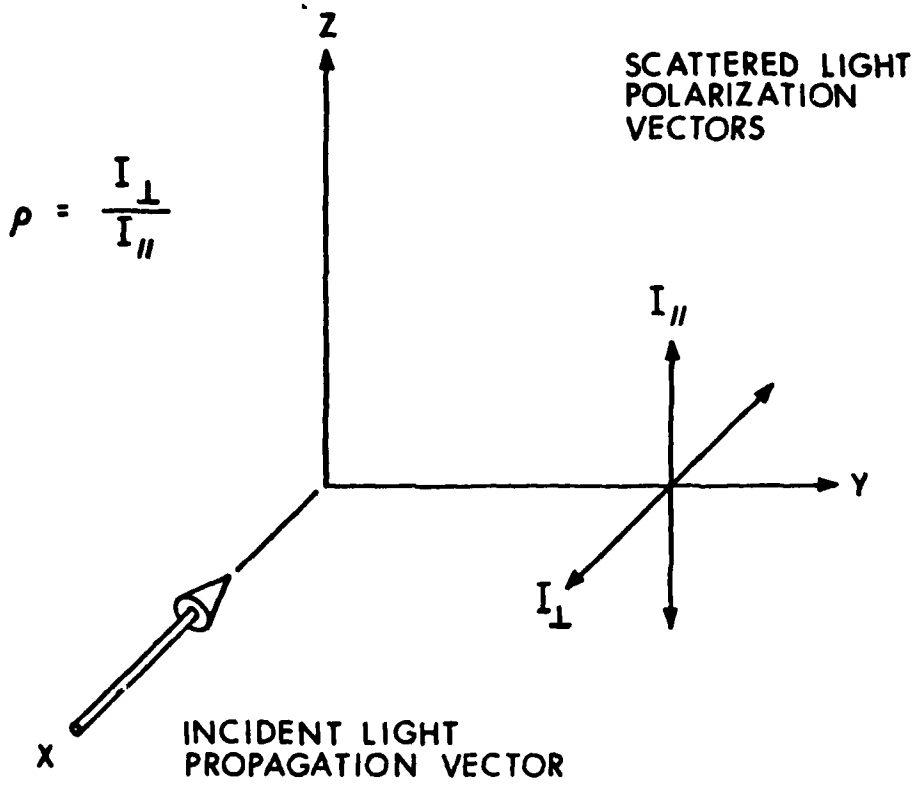

Figure 2. Definition of geometry for consideration of effects of polarization in inverse Raman spectroscopy.

bands at 2723, 2860, 2913, 2978 and 3000 cm^{-1} were observed with both lasers polarized parallel to one another. When the lasers are polarized perpendicularly, only the 2913 band, at reduced intensity, and the 2978 band remain. The authors remark that these results agree with the results of SRS, in which the degree of depolarization is low ($\rho \sim 0$) for all bands but 2978, which is strongly depolarized.

It is obvious that, strictly speaking, a quantitative calculation of the inverse Raman absorption coefficient must take into account the depolarization ratio together with the two angles describing the relationship between the polarization vectors of the two laser beams. We shall not attempt such a treatment here. Nonetheless, it is clear from the above discussion that for a Raman line of low ρ, one must be careful to maintain good parallel polarization, while for a highly depolarized line such concern is not so important. ρ values are available for many of the strong lines from standard compilations[17], and should be used as part of the criteria of experiment design.

It is also clear that any fluctuations in probe laser polarization from shot to shot could lead to irreproducible results; the insertion of an intracavity polarizing element (such as a Brewster angle plate) would appear desirable.

D. Numerical Parameters for Eq. (9).

In order to design experiments utilizing inverse Raman spectroscopy, it is desirable to be able to estimate the anticipated absorption coefficients of those compounds suspected of being present. Unfortunately, there exists little reliable quantitative Raman data, so that one must settle for order of magnitude estimates.

In particular, the lack of values of $d\sigma/d\Omega$ and particularly $\Delta\omega$ for any but a very few molecules demands that any attempt at using IRS quantitatively be carried out by calibration of the response using known concentrations of the compound under study.

1. $d\sigma/d\Omega$. That the measurement of absolute Raman cross sections is difficult is illustrated by the large error bars (30-50%) usually quoted, and the spread (factors of 2 or 3) where multiple determinations exist. The 992 cm^{-1} band of benzene is one of the most intensively investigated. A series of measurements is considered by Grun et al.[16] in conjunction with their determination using SRG. We will choose a value of 6×10^{-30} $cm^2 sr^{-1}$ as a reasonable estimate. For estimation of unmeasured $d\sigma/d\Omega$, this value can be used in conjunction with the relative intensities of Reference 17.

2. $\Delta\omega$. The subject of Raman linewidths in liquids has received little attention. Clements and Stoicheff[21] have measured values for several liquids using SRS with a HeNe laser and a Fabry-Perot interfero meter. They obtained the following results: benzene, 992 cm^{-1} : 2.15 ± 0.15 cm^{-1} ; toluene, 1002 cm^{-1} : 1.94 ± 0.07 cm^{-1} ; carbon disulfide, 656 cm^{-1} : 0.50 ± 0.02 cm^{-1}. From the figures in their paper, the lines appear to the eye to be Lorentzian in shape; the broadening mechanism is presumably molecular interactions within the liquid. Since α is proportional to $\Delta\omega^{-1}$, those bands having a narrower width would provide greater sensitivity in IRS. Unfortunately there appears to be no simple approach to estimating $\Delta\omega$.

3. N, n_S . For a given species at a particular mole fraction, the molecular concentration N (cm^{-3}) is readily obtained from tabulated density and molecular weight values[22]. Refractive indices are somewhat more problematic, since they are wavelength dependent, while generally only the values at 5890Å (from refractometry using, or corrected to, D-line radiation) are at hand[22]. However, for work with a ruby laser pumping at ω_S, the wavelength ω_L falls fairly close to the D-line region for many useful dyes (this corresponds to a separation of $\sim$ 2560 cm^{-1}). Consequently n_{5890} is probably a reasonable estimate of n_s. For many organic liquids (e.g., benzene, toluene, benzaldehyde) the value of the refractive index is close to 1.50.

4. $\rho(\omega_S)$ at focus. Significant absorption in IRS is obtained only with relative high power at ω_S. This is obtained using lasers of short pulse length and high energy, and by focussing within the sample. Now it can be shown[23] that for a laser of angular divergence θ, $f\theta$ is the beam diameter at the focal point of a lens with focal length f. Thus the area at focus is $\pi f^2\theta^2/4$, and $\rho(\omega_S)$ is given by

$$\rho(\omega_S) = \frac{4P}{\pi f^2 \theta^2} \qquad (14)$$

---

[21] *W. R. L. Clements and B. P. Stoicheff, "Raman Linewidths for Stimulated Threshold and Gain Calculations", Appl. Phys. Lett. 12, 246-248 (1968).*

[22] *Handbook of Chemistry and Physics, Chemical Rubber Publishing Co., Cleveland (1955) and other editions.*

[23] *A. DaMommio, in Fundamentals and Applications of Lasers. Volume I, Technical Education Research Center, Waco, Texas, 1976, p. I-9-17ff.*

where P is the nominal peak power of the laser. (Of course, if a lens of relatively short focal length is used, the area of the beam will vary throughout the sample length, and $\int \rho(\nu_s) d\nu$ in Eq. (5) must be considered explicitly as a function of x prior to the integration. This situation will be considered below in conjunction with the experimental results.)

E. A Numerical Estimate of α

We here calculate a typical value of α to illustrate the magnitude of the inverse Raman effect. The benzene band at 992 cm^{-1} is chosen as an example. From the preceding section, we take $d\sigma/d\Omega = 6 \times 10^{-30}$ cm^2 sr^{-1}, $\Delta\omega = \frac{\pi}{2} \times 2.15$ cm^{-1}, $n_s = n_{5890} = 1.50$, $N = 6.02 \times 10^{23} \times (0.88$ g/ml)/ (78.1 g/mole) = 6.77×10^{21} cm^{-3}. From Eq. (9),

$$\alpha = \frac{4.49 \times 10^3 \, P(\omega_s)}{\omega_s^3} \qquad (15)$$

yields α in cm^{-1} for $P(\omega_s)$ in watt cm^{-2} and ω_s in cm^{-1}.

There are several commercially available lasers suitable for carrying out IRS. We currently use a Q-switched ruby laser manufactured by Korad. Another candidate is the frequency doubled output of a Nd:YAG laser. We choose parameters pertinent to the oscillator/amplifier rig used in the NRL CARS experiments[24]. For IRS, it would be necessary to further double the 532 nm radiation or triple the original 1.064 μ, in order to pump a probe dye; this renders such a laser less attractive for IRS than a ruby, although significantly higher repetition rates (10 Hz) are achievable compared to < 0.1 Hz for the ruby.

We also consider 3 commercially available dye lasers; it would be necessary to use two of each for IRS, one narrowband and one broadband. These are a flashlamp pumped dye laser (Chromatix CMX4), a single stage nitrogen-laser-pumped dye laser (NRG DL-0.03), and a nitrogen-laser-pumped dye oscillator/amplifier laser (Molectron DL-14).

Pertinent specifications of P, τ and θ, taken mostly from manufacturer's specifications, are listed in Table 1. It can be seen that fast time resolution is available with all the lasers, except possibly the CMX4 which has a 1 μsec pulse length. A lens of focal length 10 cm is used to calculate values of $P(\omega_s)$ for comparison (however, see below). The wavelengths of the ruby and doubled Nd:YAG lasers are fixed; that of the tunable dye lasers is taken as the maximum gain wavelength for the stable, convenient, and powerful dye Rhodamine 6G.

---

[24] J. W. Nibler, J. R. McDonald and A. B. Harvey, "CARS Measurement of Vibrational Temperatures in Electric Discharges", Opt. Comm. 18, 371-373 (1976).

TABLE 1. OUTPUT CHARACTERISTICS OF SOME COMMERCIALLY AVAILABLE LASERS

LASER	PULSE LENGTH nsec	PEAK POWER P, WATTS	FULL ANGLE DIVERGENCE, θ, mrad	P AT FOCUS, MW/cm^2, for f=10 cm	λ_s (nm)	α cm^{-1}	$e^{-\alpha}$	$e^{-10\alpha}$
Korad ruby	20	100×10^6	6	3.5×10^4 [c]	694	53[c]	0[c]	0[c]
Nd:YAG	20[a]	2×10^6 [a]	4[b]	1.6×10^3	532	1.1	0.33	2×10^{-5}
CMX4	1000	6×10^3	2	19	590[d]	0.018	0.98	0.84
NRG	5	70×10^3	8	14	590[d]	0.013	0.99	0.88
DL14	5	60×10^3	1	760	590[d]	0.70	0.50	10^{-3}

[a] Ref. 24

[b] Estimated

[c] Unrealistic practically; see text.

[d] See text.

The calculated values of α are listed, together with the fraction of the incident probe beam transmitted through a 1 cm cell ($e^{-\alpha}$) and a 10 cm cell ($e^{-10\alpha}$); variation of the beam size with distance has been neglected.

A 1 cm path length is probably the maximum which can be used in an actual detonation experiment. From Table 1, it appears that only the ruby, Nd:YAG and dye oscillator amplifier provide sufficient absorption. The ruby laser is far more effective in principle, although (see below) its high power cannot be fully utilized. It should be noted that the use of an f=5 cm lens, feasible for the CMX4 and NRG lasers, would increase α by a factor of four and yield the values: $e^{-\alpha} = 0.93$ and 0.95, $e^{-10\alpha} = 0.49$ and 0.59, respectively.

Aside from cost and availability considerations, the nitrogen-laser-pumped oscillator/amplifier dye laser appears much superior to the Nd:YAG. The values of α are comparable. A portion of the nitrogen laser may be split off to simultaneously pump the broadband dye laser at ω_1, without need for further frequency doubling. The repetition rate is faster (60 Hz) and thyratron triggering is standard.

F. Window Damage: A Severe Limitation

The power density at the focus of the ruby laser is nominally (Table 1) some 35 GW/cm^2. This is beyond the threshold value for damage of cell windows, and the beam cannot in reality be focused so tightly. This problem poses a severe limitation on the maximum attainable power density, well below that quoted in Table 1, and a concomitant limitation on α and the sensitivity of IRS.

We have performed (not always intentionally) a number of experiments illustrating and illuminating this problem. We have been notably unsuccessful in focusing a 1 J laser pulse within a 1 cm cell using a lens with f=12 cm. From measurements of beam diameters in air, it appears that our cell windows can usually tolerate measured average power densities of ~ 250 MW/cm^2 but unfailingly shatter above ~ 750 MW/cm^2. On this basis, it appears that a typical damage threshold is ~ 500 MW/cm^2 as we measure it. From other measurements, however, it is clear that the ruby beam is not always homogeneous. Rather there can exist within it small regions of considerably higher power density, so that the window can be subject to much larger local values than the 0.5 GW/cm^2 measured as an average over the entire beam.

Eckbreth et al.[4] also discuss the problem of optical component damage, quoting studies which found surface damage thresholds in the 10-20 GW/cm^2 range, at the ruby wavelength. This is in reasonable accord with our results, under the presumption that local 'hot spots' in the beam actually cause the fracture.

This poses an upper limit on the power densities attainable in an experiment involving a condensed phase which must be contained. For a 1 cm cell, $P(\omega_s)$ at focus is not much different from that at the window, 0.5 cm away, through which the beam must pass. If we adopt 1 GW/cm^2 as the maximum tolerable power density, then for the 992 cm^{-1} band of benzene and the ruby wavelength, one has an $\alpha_{max} \approx 1.5$, yielding $e^{-\alpha\ell} \approx 0.22$.

We can also examine these values in terms of sensitivity. Optimistically, one might detect 1% absorption on a single shot using suitable differencing techniques (see Reference 1 and below), so that $\alpha\ell \sim 0.01$. Eq. (15) is rewritten to reflect a mole fraction X less than 1.

$$\alpha\ell = 4.5 \times 10^{-3} P(\omega_s)\, X/\omega_s^3. \qquad (15a)$$

Using 1 GW/cm^2 at 694 nm, 1% absorption corresponds to $X = 0.007$ for benzene in a path length of 1 cm, and 0.1 of this amount for $\ell = 10$ cm.

In the case of gas phase studies, one may often place the cell windows close to the lens and far from the focal point, so that the power density at the window is considerably less than that at focus. For a condensed phase system, the window must be closer to the reacting mixture in order to contain it. Even if some means could be devised to permit a more remote window location, power densities much higher than our nominal 1 GW/cm^2 can cause effects within the liquid. On several occasions we have observed reaction (sometimes of an explosive nature) within cells containing benzaldehyde-toluene mixtures experiencing sharp focusing of the ruby laser. This is presumably caused by multiphoton-induced chemical reactions. Results of the recent intense and widespread experimental investigation of laser-induced chemistry (see, e.g., Ref. 25) suggest that such processes are indeed likely at these power levels. Consequently, in work with condensed phases at least, even some innovative cell designs may not permit the use of power densities much above 1 GW/cm^2.

G. α for a Nonhomogeneous Pump Beam

The amount of absorption is an exponential function of α, and hence of the pump laser power. Thus a spatially inhomogeneous ruby beam combined with a homogeneous dye probe will in general yield a degree of absorption different from that obtained from a homogeneous pump beam of the same total pulse energy and overall beam size. That is, the average of the function $e^{-\alpha\ell}$ over the beam cross section is not the same as the function of α averaged over the cross section:

[25] *Symposium on Laser-Induced Chemistry, American Chemical Society Meeting, Anaheim, California, March 1978.*

$e^{-\alpha l} \neq e^{-\langle \alpha \rangle l}$ (17)

As a simple numerical example, consider the case illustrated in Figure 3. A pulse of power P irradiates a region of radius r, so that the average power density is $P/\pi r^2$. If, however, half the power is concentrated in a circle of half the radius, and the other half spread out over the remainder, the density is three times as large in the smaller circle.

For small enough αl, so that $e^{-\alpha l} \approx 1 - \alpha l$, there is no difference. However, the inhomogeneous beam in Figure 3 will yield a concentration too low by ~ 10%, for $e^{-\alpha l} \sim 0.4$, and too low by 50% for $e^{-\alpha l} \sim 0.13$. In reality, there likely is a more pathological power distribution than that indicated in Figure 3, and then the discrepancies are larger.

Yeung[15] addresses the issue of beam homogeneities and draws the conclusion that if one of the beams is homogeneous, this will average out spatial fluctuations in the other. His reasoning is incorrect. He considers the interaction as the product of the two beam intensities, whereas as described above, the pump laser intensity enters in exponentially. Only for small absorption, where the exponential can be replaced by a linear function, is Yeung's approach valid*. Pump laser inhomogeneities can cause errors if not accounted for. However, because the dye laser intensity enters linearly, variations in its spatial profile are no problem as long as the pump laser beam is homogeneous.

IV. EXPERIMENTAL DETAILS

Vonlolle assembled and tested the basic apparatus used in the present experiments. The sole addition (albeit a major improvement) made by ourselves was the addition of an OMA. We here describe the basic experimental setup, and also briefly summarize Vonlolle's findings[1].

A. Experimental Apparatus

Figure 4 shows the arrangement for the transverse pumping mode** used for nearly all our experiments. A Q-Switched Korad ruby laser produces pulses of ~ 2J energy and 25 nsec duration. A portion of this 6943Å radiation is frequency doubled by an ammonium dihydrogen phosphate crystal. A dielectric beam splitter reflects the remaining visible radiation and transmits the ultraviolet. The 3971Å radiation is incident upon the face of a square quartz cuvette, such as those normally used for ultraviolet spectrophotometry. This cuvette contains a dye, typically of the rhodamine

---

*Since, for a linear function $f(x)$, $\langle f(x) \rangle = f(\langle x \rangle)$.

**I.e., the beam pumping the dye is perpendicular to the dye laser beam.

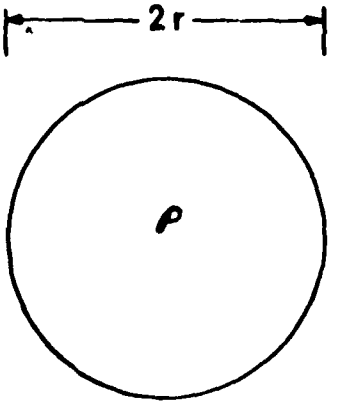

POWER DENSITY $\frac{P}{\pi r^2}$

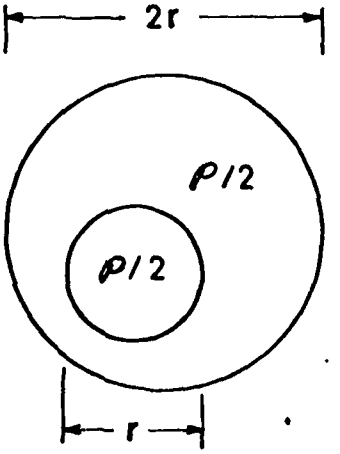

POWER DENSITY, SMALL CIRCLE $\frac{2P}{\pi r^2}$

POWER DENSITY, LARGE CIRCLE $\frac{2}{3}\frac{P}{\pi r^2}$

Figure 3. Schematic illustration of power density for (top) a homogeneous beam, (b) a beam with a hot spot containing half the power within half the radius.

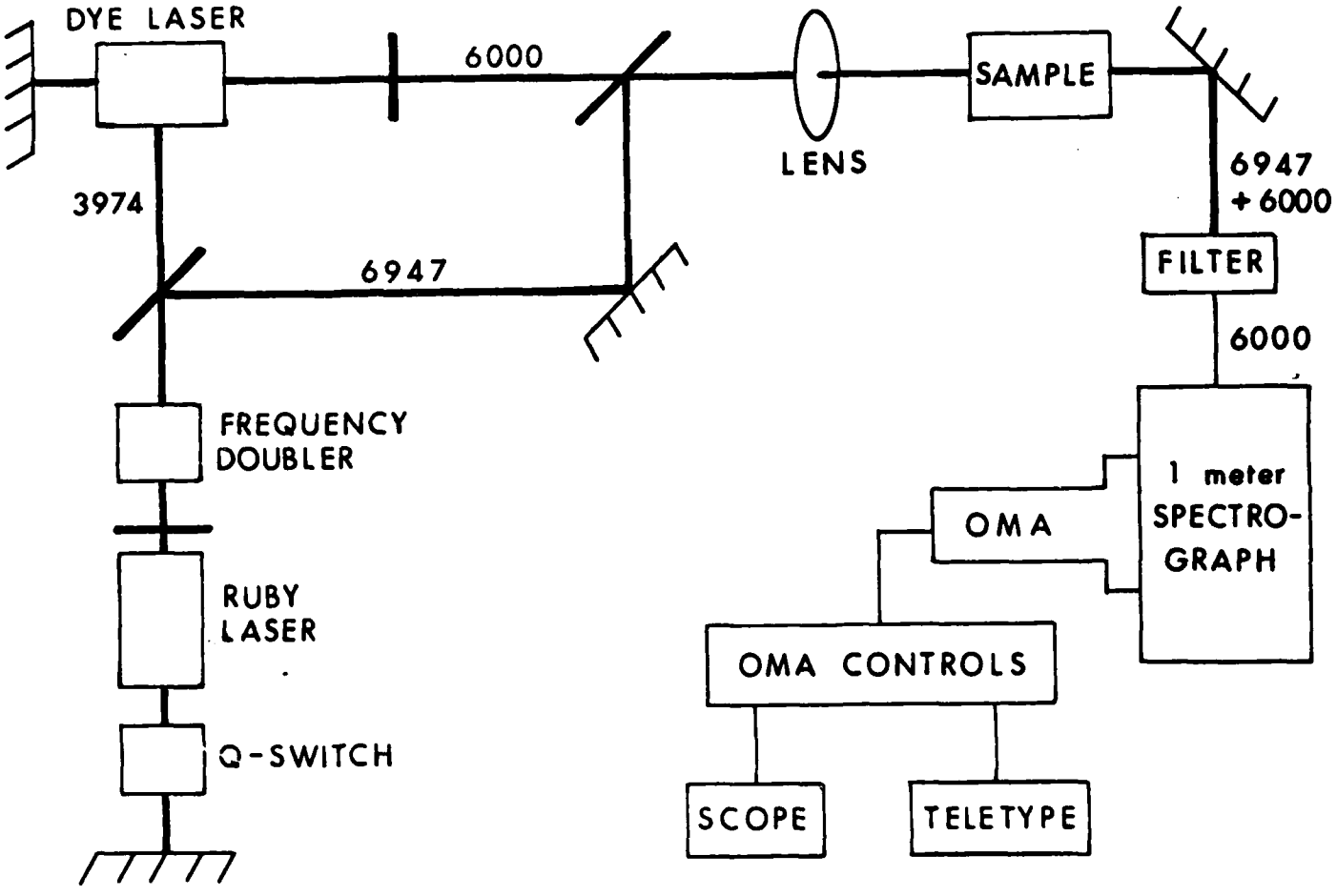

Figure 4. Schematic diagram of apparatus. Numerical values are wavelengths involved, in Å. The dye laser is actually broadband in the region of 6000 Å.

tally, which lases within the cavity formed by a totally reflecting rear mirror and a transmitting (30% reflectivity) output mirror*. Although the cuvette face is oriented at approximately Brewster's angle with respect to the dye beam, it does not produce a high degree of polarization. There are no tuning elements within the dye laser cavity, and the spectral profile is thus broad. Various peak wavelengths are obtained by using different dyes or different concentrations of the same dye, following Venkolle's investigation[1] of useful wavelength ranges for this laser. In addition, we have used rhodamine 640 (Exciton, Inc, Cleveland) for small frequency shifts; in some cases mixing the 640 with rhodamine 6G increased the pumping efficiency** and/or provided a broader total wavelength coverage, depending on the relative concentrations.

The dye laser radiation was then mixed with the 6943Å beam using another dielectric beam splitter. The dye and ruby wavelengths are close enough that some ruby light leaked through this beam splitter; this transmitted beam was often used to monitor the ruby laser pulse shape using a fast photodiode and storage scope, or its energy using a calorimeter and memory voltmeter. The ruby pulse energy at the cell was ~1J.

A lens then focussed the collinear beams through the sample cell. These were constructed in several total path lengths by cementing quartz windows onto the ends of glass tubing ~3cm diameter, with a filling port attached. Alignment of the ruby and dye laser beams through the cell was critical; a small helium-neon laser shining through the ruby rod was invaluable for this purpose.

A 6943Å rejection filter following the sample removed most of the ruby light. The dye beam (and some remaining ruby) were further attenuated using neutral density filters, and directed to the entrance slit of a 1-meter Jarrell-Ash spectrometer used as a spectrograph. An entrance slit width of 50 μ was typically used, providing ~ 0.7Å or $2cm^{-1}$ full width at half maximum for isolated narrow lines from a Hg lamp. The observed widths of the bands was typically three to four times this value.

In the first stages of our experiments, detection was by means of Kodak 103F photographic plates placed at the exit plane of the spectrometer. (For set up and exploratory surveys, Polaroid type 52 film sheets were used). After development, the plates were read using a recording microdensitometer. This proved (unsurprisingly) to be a tedious and time-consuming method; furthermore, the results discussed in Section VA suggest that the use of photographic detection leads to serious limitations in reproducibility.

*The cavity length is ~ 18cm, permitting only ~ 75 round trips during the pumping pulse duration.

**Not an important concern here since we always had ample dye laser intensity.

The addition of the OMA thus proved to be a most welcome and useful improvement. Ours is the original version (now referred to as "OMA-1") from the Princeton Applied Research Corporation, with a silicon intensified target detector head. When used at the exit plane of the 1-meter spectrometer, the 0.5" spread of the diode array covers $\sim$ 250 to 300 cm^{-1} at the wavelengths used, thus including all or nearly all of the broadband dye laser spectral profile. The diodes have a 25 μ spacing so that they are not the limiting resolution factor for a 50 μ slit width. The OMA control console was connected to an oscilloscope for survey readout, and to a teletype for numerical hard copy. The console digital display was used for some of the data taking, with appropriate channel selection by inspection of the scope display. Because of internal trigger delay aspects of the OMA, it was necessary to begin the OMA diode scan before firing the ruby laser. This was accomplished by construction of a small interface circuit, so that a signal from the OMA tripped the ruby Q-switch.

B. VonHolle's Results

VonHolle carried out measurements on three bands of the benzene molecule, at 3067, 2949, and 992 cm^{-1}, and on a band of nitromethane at 920 cm^{-1}. Data were taken in mixtures ranging from pure CH_3NO_2 to about 35 mole per cent C_6H_6. A reasonably straight line* was obtained for the relative absorption vs. $X(C_6H_6)$. Some variation in CH_3NO_2 absorption was observed for X = 0.75 to 0.95 although the data do not, over this small range, define a clean straight line without a separate constraint of zero absorption at zero concentration. Nonetheless, the results demonstrate at least semiquantitative utility; a lower limit of sensitivity for C_6H_6 would appear about X = 0.1 in this work.

VonHolle carried out a survey inverse Raman spectrum of a thermally decomposed liquid propellant containing (among other ingredients) hydroxyl ammonium nitrate and isopropyl ammonium nitrate. After refluxing and heating, the propellant exploded. Both the original liquid and the decomposed liquid were probed. In the pure liquid, a strong band at 1050 cm^{-1} (with a shoulder at 1057 cm^{-1}) was found and assigned to ν_1 of the nitrate ion. The inverse Raman spectrum of the decomposed propellant was considerably weaker, necessitating the use of a differencing technique. A portion of the dye laser radiation was split off prior to entering the sample, and focussed on a different vertical position on the spectrometer slit as a reference beam. Subtraction of this reference from the profile of the dye which had passed through the sample revealed a number of spectral features more difficult to discern in the original spectrum (see below). Notably, the nitrate band was considerably reduced from the original propellant. In addition, both N-O and C-N bands of the nitro group were present, indicating the formation of (perhaps aliphatic) nitro compounds during the decomposition.

Except for some residual absorption at zero mole per cent, a strange problem we encounter as well.

The primary source of noise in Vonlolle's spectra is attributed to the existence of intracavity mode structure in the dye laser. This presumably varies randomly from shot to shot, but if it is the major noise source, then the single-shot differencing technique Vonlolle used should be quite applicable. In this way, he was able to discern absorption of ~ 2% through his cell*. He found somewhat cleaner mode structure using a longitudinal pumping scheme, but at the expense of laser intensity.

Vonlolle concluded that his results demonstrated the potential of broadband, rapid single-shot IRS as a probe of explosive reactions. Our agreement with his conclusion has formed the starting point of our investigation of the quantitative aspects of IRS in this mode.

V. EXPERIMENTAL RESULTS

The primary focus of the experiments was to test the reproducibility of the inverse Raman signals, and to estimate uncertainties (systematic and random) anticipated in using such signals as a measure of concentrations in solutions. The experiments were initially carried out using a photographic plate for detection; the primary conclusion from this phase of the work was that electronic detection would be both much easier and more accurate.

Nearly all of the data taken (and all of that reported here) has been on the benzaldehyde** molecule either neat or in solution with toluene. The peaks utilized for measurement are at 1597 cm^{-1}, and are referred to below by these numerical designations.

A. Photographic Measurements

Two series of runs were made on solutions of 20 and 50 mole percent BZD in toluene. The 10cm path length cells were used for all runs. Because of problems in associating the absolute absorption coefficient to the BZD density, all measurements were made using as a calibration the same cell filled with pure BZD. The runs with neat BZD were generally alternated with those of the mixtures, to compensate for longer term drift in the laser power.

In the first series, the total absorption was of the order of 20-25% for pure BZD. The fractional absorption for the mixtures was consistently higher than the value of the corresponding concentration. There existed a smooth gradient in total optical density (dye laser intensity) in the direction parallel to the slit, perhaps indicating improper spectrometer alignment. The fractional absorptions varied with the position, in this direction, measured by the microdensitometer, and were systematically lower for 1597 than for 1701 (see Table 2). This is somewhat surprising

---

*Assuming a δ value of 1.4 for his plates, see reference 1.

**Referred to below as BZD.

TABLE 2. FRACTIONAL ABSORPTION, AT VARIOUS CONCENTRATIONS, FOR EARLY PHOTOGRAPHIC RUNS

α RATIO FOR SPECIFIED CONCENTRATIONS	PLATE POSITION	1701	1597
α(50) /α(100)	a	.88 ± .17	.48 ± 14
	b	.67 ± .03	.49 ± 4
	c	.79 ± .14	.69 ± 14
	d	.63 ± .06	.59 ±.09
α(20) /α(100)	a	.28 ± .02	.19 ±.01
	b	.50 ± .03	.35 ±.03
	c	.52 ± .09	--
	d	.38 ± .03	.32 ±.05
α(20) /α(50)	a	.32 ± 6	.40 ±.11
	b	.75	.71
	c	.65	--
	d	.59	.54

Fractional absorption, at various concentrations, for early photographic runs. Plate position a is that of highest exposure, while d is the lowest. Errors are simple averaging over multiple runs; the lack of an error bar means only one such run was made.

TABLE 3. FRACTIONAL ABSORPTIONS, FOR LATER PHOTOGRAPHIC RUNS

SERIES NUMBER	CONCENTRATION (X_1/X_2)	BAND	$f=\alpha(X_1)/\alpha(X_2)$	Δf	n
3	50/100	1700	.56	-	1
4			.55	-	1
5			.66	.00	2
6			.54	-	1
7			.73	-	1
12		1701	.75	-	1
		1597	.59	-	1
13		1701	.78	.15	3
		1597	.83	.11	3
14		1701	.63	.09	4
		1597	.50	.15	4
18		1701	.83	.08	3
		1597	.83	.09	3
19		1701	.65	.00	2
		1597	.68	.05	2
20		1701	.76	-	1
		1597	.54	-	1
21		1701	.88	.06	3
		1597	.87	.03	2
22		1701	.84	-	1
		1597	.66	-	1
28		1701	.58	.05	2
30		1701	.81	.04	6
31		1701	.75	-	1
		1597	.55	-	1
33		1701	.59	.04	7
34		1701	.70	.04	6
		1597	.92	.03	4
35		1701	.91	.00	2
		1597	.78	.04	2
36		1701	.59	.04	5
37		1701	.77	.00	2
		1597	.52	.02	2
	20/100				
19		1701	.30	.03	2
		1597	.21	.02	2
20		1701	.26	-	1
		1597	.33	-	1
21		1701	.31	-	1
		1597	.24	-	1
22		1701	.21	-	1
		1597	.26	-	1
30		1701	.35	-	1
		1597	.32	-	1

TABLE 3. FRACTIONAL ABSORPTIONS, FOR LATER PHOTOGRAPHIC RUNS (Cont'd)

SERIES NUMBER	CONCENTRATION (X_1/X_2)	BAND	$f=\alpha(X_1)/\alpha(X_2)$	Δf	η
31		1701	.32	-	1
		1597	.25	-	1
34		1701	.40	.04	5
		1597	.33	.03	2
35		1701	.67	.04	2
		1597	.58	.02	2
37		1701	.46	.01	2
		1597	.32	.06	2
	20/50				
19		1701	.46		
		1597	.42		
20		1701	.34		
		1597	.61		
21		1701	.35		
		1597	.28		
22		1701	.25		
		1597	.39		
30		1701	.44		
		1597	.40		
31		1701	.64		
		1597	.46		
34		1701	.57		
		1597	.36		
35		1701	.74		
		1597	.74		
37		1701	.59		
		1597	.61		

Fractional absorptions, for later photographic runs. η is the number of runs in each series; Δf is from simple averaging only.

in view of the fact that toluene has a Raman-active band at [illegible] and might be expected to lead to systematic errors in this direction for the other BZD band.

A second series of runs, made essentially in plate position [illegible], was carried out over a period of two months, often with multiple runs on one day, to assess reproducibility. The rather disappointing results of this exercise are collected in Table 3.

From this experience, we conclude that inverse Raman spectroscopy with photographic detection is not well suited for quantitative concentration measurements on a single shot basis. Part of the problem may lie in the known problems of using photographic plates for intensity measurements; linearity (plate optical density vs. incident light intensity) is expected over only a small range. The short "exposure times" corresponding to the laser pulse length may aggravate this as well. Indeed, an earlier study[26] investigated the dependence of the IRS absorption coefficient α on the power of the pumping ruby laser. There, it was found that the anticipated proportionality was not obtained when photographic detection was used, but good agreement was achieved with photoelectric detection.

In view of these difficulties, coupled with the time-consuming and tedious method of using photographic plates, a photoelectric technique is decidedly preferable. The use of the OMA in the present work has vastly increased the quantity as well as the quality of the results. Undertaking a project such as this without an OMA is, we feel, not cost-effective when considering its price tag of ~ $17K.

B. Early OMA Concentration and Reproducibility Runs

Our early (and only extensive) series of measurements of the absorption in solutions of BZD in toluene did not appear to greatly reduce single-shot scatter but significantly improved the linearity. Figure 5a shows a series of runs in which the quantity $\alpha/P(w_s)$ for 1701 (see Eq. (9)) is plotted vs. mole fraction BZD. For the total of 13 shots, $P(w_s)$ varied within a range of ±7%. Again, some residual absorption is seen in neat toluene, and the scatter is considerable. However, the fractional absorption at 20 and 50 mole per cent is considerably closer to 20 and 50 per cent of that of pure BZD.

The average values for these runs are impressively more accurate than the individual points. Figure 5b shows the averages, excluding the X=0 points and the one spuriously low point for X=0.2. In retrospect, we know that the ruby rod in use at that time may have been deteriorating, leading to some scatter in the results. Our later data on other aspects

---

[26] *Y. Tsunoda, "Inverse Raman Effect of Some Organic Liquids", Jap. Journ. Appl. Phys. 11, 1203-1207 (1972).*

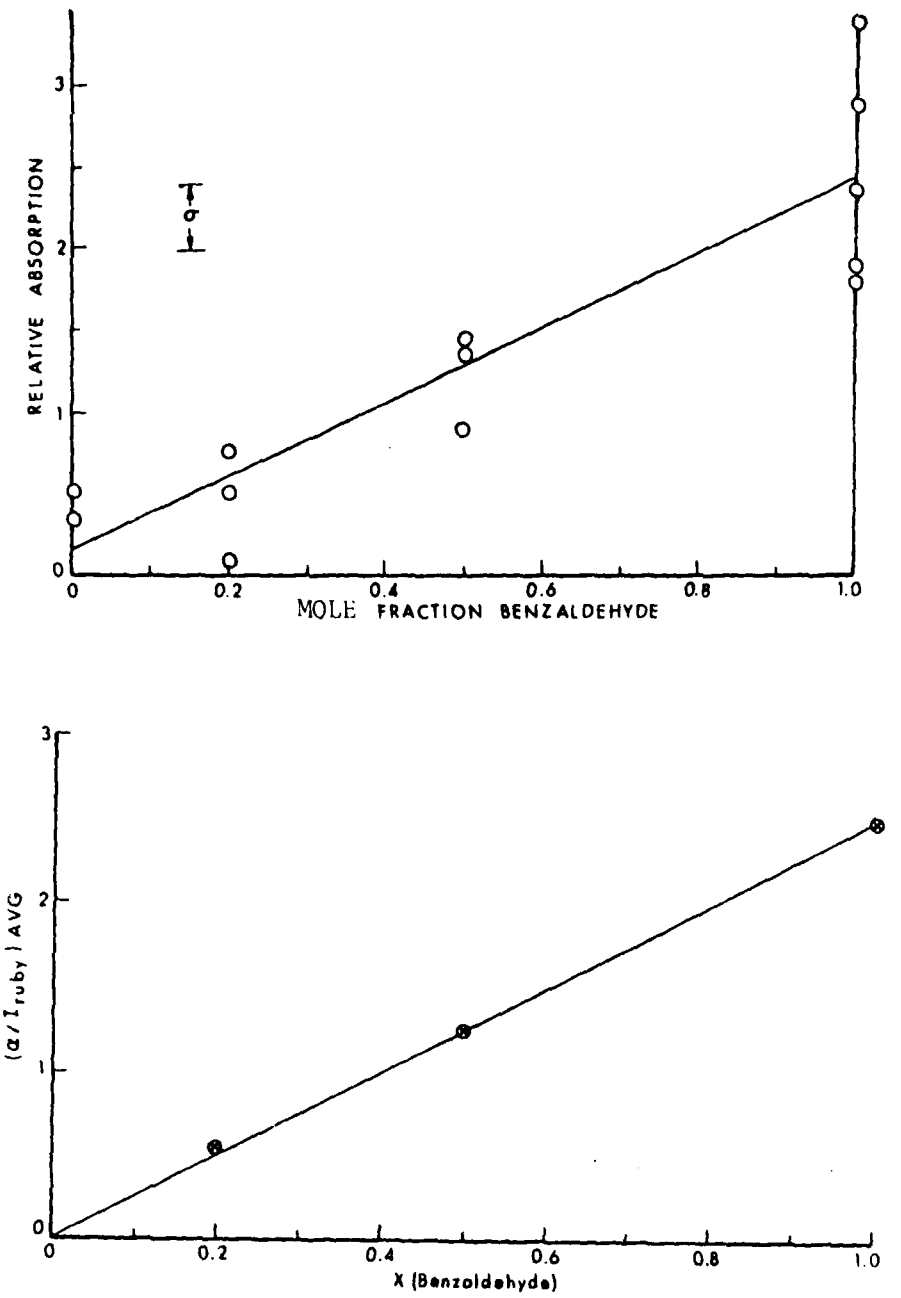

Figure 5. Relative absorption at 1701 cm^{-1}, normalized to the value at mole fraction 1. (a) Single shot experiments: each point represents one single shot determination. (b) Averages of values in (a), excluding the anomalously low point at X = 0.2.

of the α vs $P(w_s)$ (section VI.) suggests better behavior than is implied in Figure 5a.

A series of runs on 1701 of pure BZD were carried out to assess reproducibility. In Table 4 are listed α, $P(w_s)$ and their ratio. Again one obviously spurious value (1.42) can be noted. Not including this value, α averages to ±13% and $\alpha/P(w_s)$ to ±10%.

C. Absorption as a Function of Ruby Intensity

Two series of runs were made, again in pure BZD at 10 cm path length, on both 1597 and 1701. In these, filters were used to vary the 6943Å intensity at the cell over a factor of about five, while maintaining the (here irrelevant anyway) dye laser intensity constant. The results are presented graphically. Plotted is α_{1701} vs $P(w_s)$, α_{1597} vs. $P(w_s)$, and α_{1701} vs α_{1597}.

Figure 6 shows the first set of runs made in this manner. The scatter can be used to gauge general single-shot reproducibility as well as the dependence of α on $P(w_s)$. Figure 7 displays plots of α_{1701} vs α_{1597} for a further series of runs.

The slopes of these curves may be compared with that expected on the basis of Eq. (9). We use the intensities of published SRS spectra[17], and correct for the wavelength dependence corresponding to the argon ion laser used there* to obtain $(d\sigma/d\Omega)_{1701} / (d\sigma/d\Omega)_{1597} = 0.81$. For equal $n_s \Delta\omega$ then we expect a ratio of 0.79 for these bands shifted from the ruby wavelength. While the points in Figures 6c and 7b are reasonably described by this ratio, the runs shown in Figure 7a show $\alpha_{1701} > \alpha_{1597}$. We can offer no explanation for this particular set of results.

D. Focussing Considerations

The diameter d of the focussed laser beam varies more or less linearly with distance from the focusing lens, and α is proportional to d^{-2}. Since the amount of absorption varies as $e^{-\alpha}$, a large portion of the absorption must arise in a small path length near the beam focus. We have carried out a qualitative experiment comparing the absorption from a 2.5-cm-cell with that of a 10-cm-cell. If the 2.5-cm-cell occupies the same position as the front** 2.5 cm of the 10-cm-cell, we still obtain about 60% as much absorption as with the 10-cm-cell. If the 2.5-cm-cell is closer by 3 cm to the lens, however, no absorption is obtained, demonstrating a rapid variation with spectral power density. When the 2.5-cm-cell is positioned so that the ruby pulse is focussed at its center, we obtain significantly less absorption (see Figure 8). This

---

We have not found information in Ref. 17 describing the spectral response of the detector.

**Closer to the lens.*

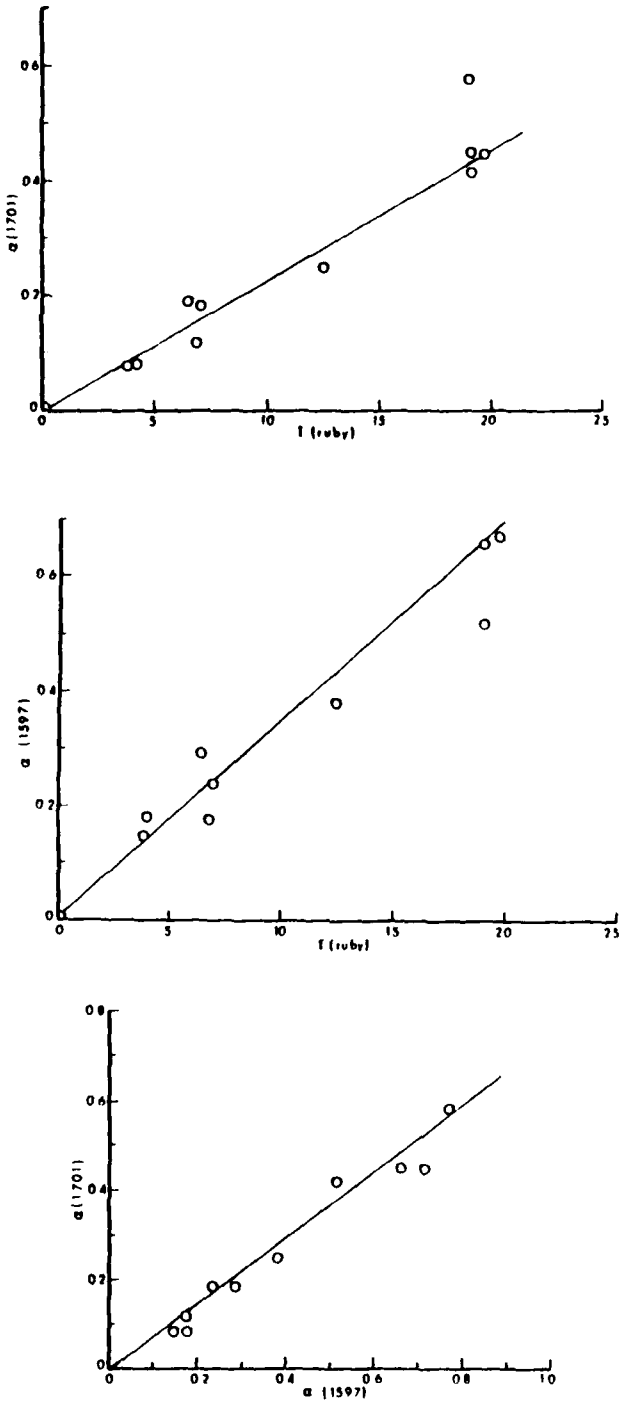

Figure 6. (a) Absorption at 1701 vs. ruby laser power. (b) Absorption at 1597 vs. ruby laser power. (c) Absorption at 1701 vs. absorption at 1597 for the same series of shots. These are all single-shot values.

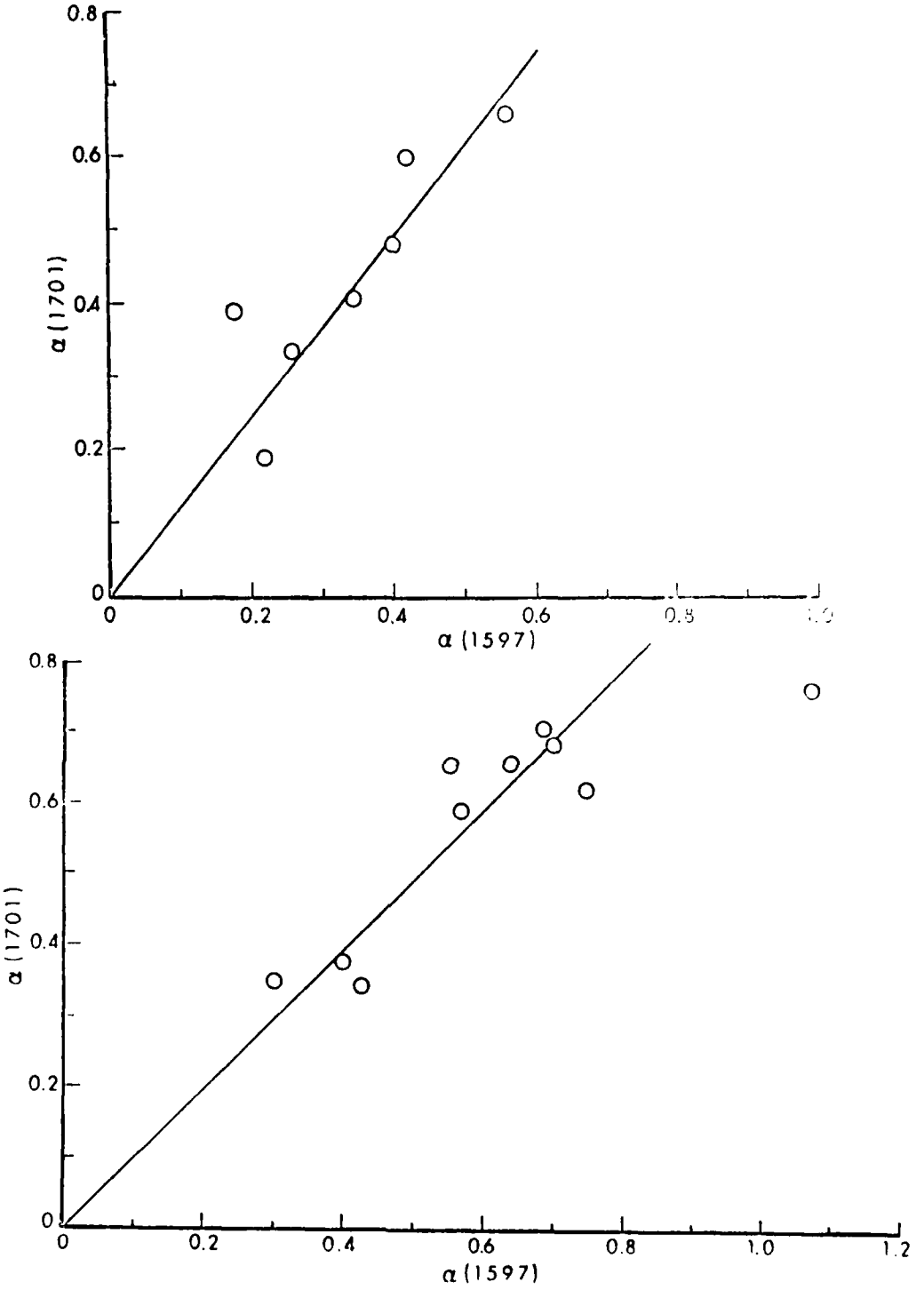

Figure 7. Absorption at 1701 vs. absorption at 1597, for a series of ruby laser powers. (a) and (b) show two separate series of runs.

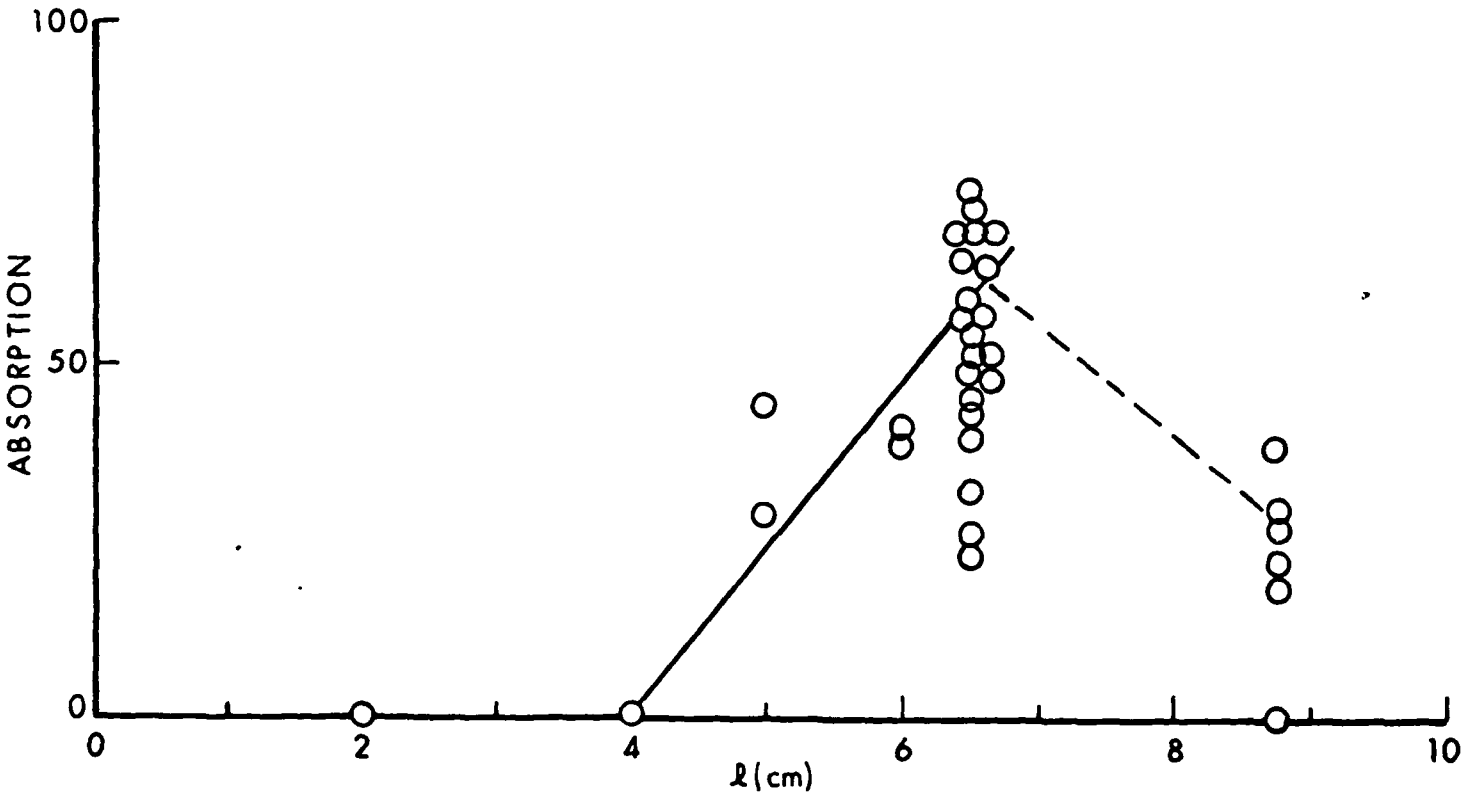

Figure 8. Absorption in the 2.5 cm cell, plotted as a function of the distance from the focusing lens. Numerical values of absorption are percentages of the absorption obtained for the 10 cm cell under the same conditions.

TABLE 4. ABSORPTION, RELATIVE LASER INTENSITY, AND THEIR RATIO FOR A SERIES OF RUNS ON BZD IN A 10 CM CELL

α	$P(\omega_s)$, ARBITRARY UNITS	$\alpha\ 100\alpha/P(\omega_s)$
0.51	20.4	2.50
0.47	20.4	2.30
0.44	18.4	2.38
0.30	21.3	1.42
0.44	20.2	2.17
0.36	18.0	2.00
0.40	19.4	2.06
0.49	18.4	2.66
0.38	17.6	2.16
0.37	17.9	2.07

somewhat surprising result may be due to such high power densities that we are appreciably populating the upper vibrational level, or the fact that the effective ruby beam diameter may here be smaller than the dye beam diameter. This would reduce the apparent absorption; also the dye beam may be focussed upon a less intense part of the ruby beam spatial profile.

Whatever the case, these results imply that the bulk of the absorption within the longer path length cell comes from a total path length* of 3-4 cm. The simple use of the path length ℓ in Eq. (6) to derive an absolute α from the per cent absorption is not warranted. We have not attempted a quantitative treatment of the data in Figure 8, as the BZD itself changes the effective focal length of the lens, but in Section V F we consider in a simplified fashion the effects of beam diameter varying with position.

It was largely during these runs (and similar ones with a 1 cm cell) that we gained most of our experience concerning window damage thresholds discussed in Section III F. Given that experiments on explosive materials will be carried out in necessarily short cells, it is noteworthy that the qualitative results of Figure 8 show that a 1 cm cell should produce considerably more absorption than a comparison of $e^{-\alpha}$ and $e^{-10\alpha}$ would imply.

E. Effects of Polarization

The effects of polarization are discussed in Section III C. Both the 1701 and 1597 bands of BZD are partially polarized[17]: $\rho_{1701}=0.4$ and $\rho_{1597}=0.3$. Thus one would expect some dependence on relative polarization of the ruby and dye lasers.

The ruby laser is polarized in a vertical direction and normally the dye laser is essentially unpolarized. Here, the dye laser was operated unpolarized, and polarized horizontally and vertically. The results, listed in Table 5, are not particularly conclusive. They suggest little dependence on polarization; $\alpha_{1701}/\alpha_{1597}$ is noticeably higher for the vertical mode as might be expected from the ρ values.

F. Absolute Inverse Raman Absorption

In Section III E, Eq. (15), a numerical estimate of α was given in terms of the laser power and Raman shifted frequency. We here compare our typical observed values of 30% absorption through a 10 cm path cell (of BZD) with that predicted by the considerations of Sections III D and III E. Values of $d\sigma/d\Omega$, $\Delta\omega$ and n_s for benzene are used in the absence of such data for BZD. Polarization is neglected. We need experimentally the laser pulse energy, the focussed beam area, and the effects of varying diameter through the cell.

*Using approximate values of $e^{-2.5\alpha} \sim 0.3$ and the 60% ratio.

TABLE 5. EFFECTS OF POLARIZATION

Run	POLARIZATION	$P(\omega_s)$	α_{1701}	α_{1701}/P	α_{1597}	α_{1597}/P	$\frac{\alpha 1701}{\alpha 1597}$
a	N	20.5	0.79	3.85	0.85	4.16	0.93
b	N	20.1	0.81	4.03	0.94	4.69	0.86
c	V	19.8	1.00	5.04	0.96	4.86	1.04
d	V	-	0.83	-	0.76	-	1.09
e	H	19.4	0.55	2.84	0.78	4.04	0.71
f	N	19.6	0.39	1.99	0.59	3.00	0.66
g	V	19.0	0.51	2.69	0.53	2.78	0.96

Effects of polarization. P and α/P are in arbitrary units.

1. Pulse energy. This was measured using the optics and windows of the experimental setup and found to be typically 0.7J/pulse at the cell. Little if any ruby light was removed by the BZD within the cell, although the mirrors, the lenses and cell windows attenuated the pulse over 50% from its nominal 2J value.

2. Beam diameter at focus. This in the experiment is considerably larger (3 mm, from burned holes in used sheets of Polaroid film) than that calculated (0.7 mm) using Eq. (14) and the angular divergence quoted by Korad.

3. Effects of focussing. We consider a cell of length $2\ell_o$ (≈10cm) (see Figure 9). The beam radius decreases linearly from a value r_o at the entrance window at x=0 to some minimum radius r_m at $x=x_m$. For a lens of diameter 2.5 cm and focal length 12 cm, as used in the experiments, and focussed at $x=\ell_o$, r_o=0.52 cm and r_m will then be 0.15 cm.

Now $\alpha = c \int dx/A(x)$, where c is some constant and A the beam area as a function of x, $A = \pi[r(x)]^2$. If we carry out this integral for the geometry exhibited in Figure 9, we find

$$\int_o^{2\ell_o} \frac{dx}{A(x)} = \frac{2\ell_o}{\pi r_m^2} \left\{ \frac{r_m^2}{r_o^2} \left(\frac{2r_o}{r_m} - 1 \right) \right\} . \qquad (18)$$

Were the cell homogeneous in radius r_m and of length ℓ_o, the value length ÷ area would be $2\ell_o/\pi r_m^2$. Thus the term in brackets in Eq. (18) represents the effective difference in area for the focussing geometry of Figure 9. For our parameters, it has the value 0.49, i.e., the effective ruby intensity is about half of what it would be for a beam of radius r_m constant through the cell.

4. Absolute α. We thus have a pulse energy 0.7J, a pulse duration 25 nsec, and an effective area of 0.071/0.49 cm^2, for a ruby power of 190 MW/cm^2. From Eq. (14), with ω_s = 1597 cm^{-1}, $\alpha = 1.10 \times 10^{-9}(\omega_s)$ or here α = 0.2. For a 10 cm path length, this implies 12% transmission; for a 3.5 cm path length 48%. In view of uncertainties in $d\sigma/d\Omega$ and $\Delta\omega$ for BZD itself, we feel we obtain experimentally a value of α in reasonable accord with theoretical expectations.

G. Influence of Mode Structure

In our experiments, as in VonHolle's, it appears that the dominant source of noise is mode structure in the dye laser. This amounts to as much as 10% of the dye laser output and constitutes a serious limitation

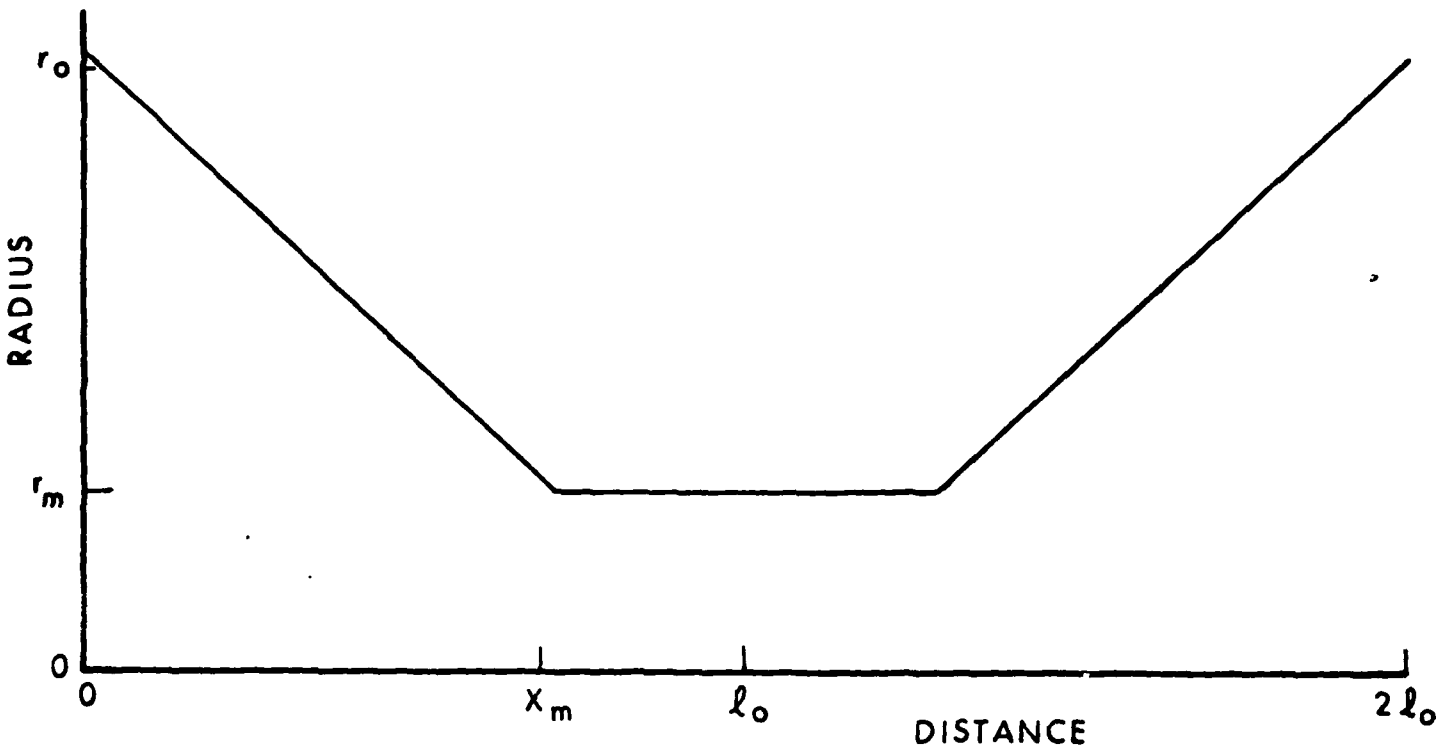

Figure 9. Defining geometry for consideration of focussing effects.

on the ultimate single-shot sensitivity. In Figure 10 is collected a number of oscilloscope photographs of the OMA output. Figure 10a shows a single shot spectrum with considerable (but not a typical) mode structure noise.

That the noise is random can be seen by averaging several shots on the OMA. Figure 10b and 10c show the results of 10 shots; 10b is the inverse Raman spectrum while 10c is the dye profile with no BZD in place. Note that in 10b a third band appears, due to the 1590 cm^{-1} band of BZD, and near the peak of the curve is absorption due to a 1660 cm^{-1} band.

The OMA can be operated in a two dimensional mode to simultaneously record the inverse Raman spectrum and a reference, as VonHolle did photographically. These can be subtracted electronically and this could be very useful for circumventing the noise problem, but we have not attempted the necessary optical alignment.

In a brief series of experiments, a longitudinal pumping scheme was tried. Here the 3971Å radiation propagates along the dye laser beam direction. VonHolle found that this improved the mode structure. We did not find significant differences for our configurations, and can claim no obvious advantages for the longitudinal scheme (which is somewhat harder to align).

VI. FUTURE DIRECTIONS

The mechanism, on a microscopic scale, by which a material undergoes detonative decomposition is in many cases a matter of considerable conjecture. This is due in large part to the severe difficulties encountered in carrying out experiments on actual detonative processes; the results are not often easily and unambiguously interpreted on the basis of molecular processes. In particular, much of the picture of the chemistry involved in detonations has evolved from measurements made upon the thermal decomposition of the same material. From products found there, one infers the species and chemical reactions important in the detonation. Of course, these two processes occur under different conditions of pressure and temperature, and on considerably different time scales. It is in general not known whether the chemistry remains the same.

It would be useful to be able to make species measurements on an actual detonation, and compare (in particular) the intermediate species observed with those found in the thermal decomposition of the same material. For such a purpose, a spectroscopic probe is desirable, in order to circumvent problems of secondary reactions occuring in such sampling techniques as chromatography. It is for such experiments that the current development of IRS is envisioned. IRS would be used first to probe the thermal decomposition itself, and then be applied to a detonative process. If similar primary or intermediate species are

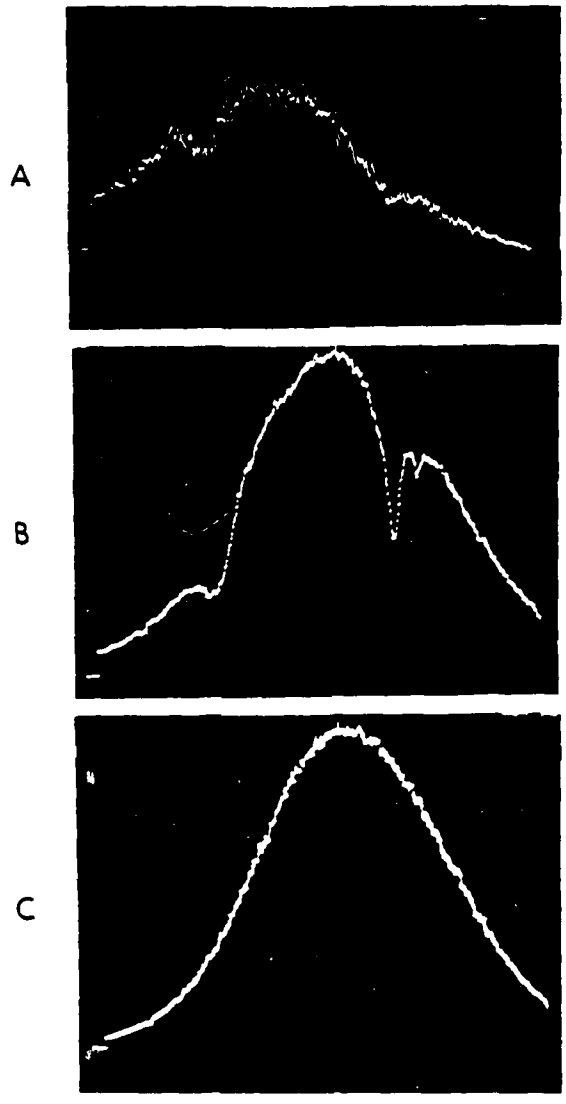

Figure 10. Oscilloscope photographs of OMA output. (a) Single-shot spectrum. The 1701 absorption is at the left, and the 1597 to the right. (b) Ten shots averaged on the OMA. Note that a third peak at slightly smaller shift is evident to the right of 1597. (c) The dye laser continuum in the absence of inverse Raman absorption. Average of ten shots.

detected, this would provide a strong indication of similar mechanisms. If there exist considerable differences, that too is of course an important result.

It should be noted at the outset that the use of single-shot IRS to study only the thermal decomposition constitutes the misuse of a diagnostic tool. The experimental results found in the present work demonstrate that single-shot, broadband IRS suffers from low sensitivity, only semiquantitative reproducibility, and requires sophisticated equipment. It is not the method of choice except where the time scales and other experimental conditions preclude the use of more established spectroscopic methods such as SRS or infrared absorption. Such conditions are present in a detonation, but the leisurely time scales involved in thermal decomposition should permit the application of these other techniques.

We have chosen, as a specific example with inherent interest, the decomposition of trinitrotoluene (TNT). The plan involves carrying out IRS studies of the thermal decompositon of TNT, and comparing the spectra with those obtained from an IRS probe of TNT detonative decomposition*.

It is necessary to perform IRS on the thermal decomposition in order to establish the spectroscopic signature sought in the detonative process. This is because the Raman spectral positions of many suspected intermediates are unknown, and intensities of even the anticipated bands cannot be at all predicted. It may be possible to ascertain some of these data by preparation of a few previously observed intermediates, and characterizing them first with SRS (for band frequencies) and then IRS (for intensities) in static cells.

In addition, it appears to us that the study of the thermal decomposition alone, by an established spectroscopic technique such as SRS or infrared absorption, would be valuable in itself as well as a useful adjunct to this work.

A. The Thermal Decomposition of TNT

We include here a brief review of some work on the thermal decomposition of TNT. This is not intended to be comprehensive in any sense, but represents a starting point from which to begin spectroscopic considerations in the experimental design.

We have not yet considered, and do not address here, the considerable non-spectroscopic aspects of carrying out the detonation experiments.

The principal well-defined products[27,31] from the low-temperature thermal decomposition of TNT* include: trinitrobenzene; 4,6-dinitroanthranil; 2,4,6-trinitrobenzaldehyde; 2,4,6-trinitrobenzyl alchohol; and 2,4,6-trinitrobenzoic acid (see Figure 11). In addition to these products, a brown powdery material (which is insoluble in benzene and does not melt at 360°C) is often formed in sizeable quantities; this is referred to as "explosive coke". These products are determined through the use of chromatographic methods.

The exact nature of the products obtained depends, however, on the conditions under which the decomposition is carried out. For example, when done using programmed-temperature pyrolysis[28] at a heating rate of 11°/min, the principal product was trinitrobenzene, although 2,4,6-trinitrobenzyl alchohol and 4,6-dinitroanthranil were also formed (quantitative results are not given in Ref. 28). However, when the TNT was decomposed for 16 hr at a constant 200°C, the observed product distribution[29] was different (see Table 5). In fact, the product mixture was considerably more complex than suggested in Table 6, since more than 25 distinct zones could be observed when the chromatographic column was streaked with alcoholic alkali[29]. Each of these probably corresponds to a single decomposition product.

The chemical mechanism involved in TNT thermal decomposition is clearly complicated** but apparently is an autocatalytic process involving

---

[27] F. C. Rauch and R. B. Wainright, "Studies on Composition B", Picatinny Arsenal, February 1969, AD-850 028.

[28] R.N. Rogers, "Combined Pyrolysis and Thin Layer Chromatography, a Method for Study of Decomposition Mechanisms", Anal. Chem. 39, 730-733 (1967).

[29] J. C. Dacons, M. J. Kamlet and D. V. Sickman, "Thermal Decomposition of TNT", NAVORD Report 6831, May 1960, AD-317 977.

[31] F. C. Rauch and W. P. Colman, "Studies on Composition B", Picatinny Arsenal, March 1970, AD-869 226.

[32] J. C. Dacons, H. G. Adolph and M. J. Kamlet, "Some Novel Observations Concerning the Thermal Decomposition of TNT", J. Phys. Chem. 74, 3036-3040 (1970); W. P. Colman and F. C. Rauch, "Studies on Composition B", Picatinny Arsenal, February 1971, AD-881 100.

*See reference 27 for a literature survey of the subject.

**References 27 and 29-32 include discussion of the kinetics and their mechanistic inferences; in particular references 29 and 30 present considerable discussion and speculation on the chemical details.

free radicals. When the CH_3 group is deuterium labelled a primary isotope effect is exhibited[32]. This together with the nature of the principal products (III - VI of Figure 11) suggests an oxidative attack on the CH_3 group as the rate-determining step. This could be either unimolecular or bimolecular; the latter route would appear favored by the formation of the alcohol, the aldehyde and the acid (IV - VI) with both ortho nitro groups intact*. The most convincing evidence for the bimolecular scheme is furnished by the fact that gas-phase TNT alone does not decompose at low temperature, strongly suggesting that the prime autocatalytic species must be generated in the liquid phase[30]. (In such a scheme, the cyclic 1,6-dinitroanthranil would be formed by cyclization of the radical formed when a hydrogen atom is stripped from the CH_3 group of the TNT30).

We reiterate that our envisioned use of IRS as a probe of the decomposition of TNT is not intended to provide unambiguous answers to these mechanistic questions. That is likely more readily accomplished, for the thermal decomposition case, using techniques such as SRS or infrared absorption (a project which appears to us worthwhile). Rather, we are considering IRS for an attack on the question: Is the mechanism (whatever it may be) similar for thermal and detonative decomposition, insofar as one may infer from the presence or lack of common species present?

B. Some Spectroscopic Considerations

Little information appears to exist in the literature concerning the Raman or infrared spectra of the compounds shown in Figure 11. A useful, and probably necessary, aspect of this project would be to first carry out SRS measurements of Raman line positions and intensities* on as many of these molecules as possible†. A further helpful intermediate step would be IRS measurements with a tunable, narrow probe (Section VI - C).

Of the trinitro compounds, there exists a pre-laser-era report[33] on the Raman spectrum of TNT itself, and more recent papers concerning the

---

[32] G. A. Shackleford, J. W. Beckman and J. S. Wilkes, "Deuterium Isotope Effects in the Thermochemical Decomposition of Liquid 2,4,6-Trinitrotoluene: Application to Mechanistic Studies using Isothermal Differential Scanning Calorimetry Analysis", J. Org. Chem. 42, 4301-4306 (1977).

[33] V. V. Shorygin, "Spectra of Combination Scattering and Special Features of the Structure of Organic Compounds", Zhur. Fiz. Khim. 22, 1409-1418 (1948).

* Although they could also be formed in the unimolecular scheme with rapid transfer of a hydrogen for a NO_2H group.

† This is also a necessary precursor to directly probing the thermal decomposition using SRS.

‡ TNT and trinitrobenzene are available commercially on a routine basis, but the other compounds would need to be synthesized for the purpose.

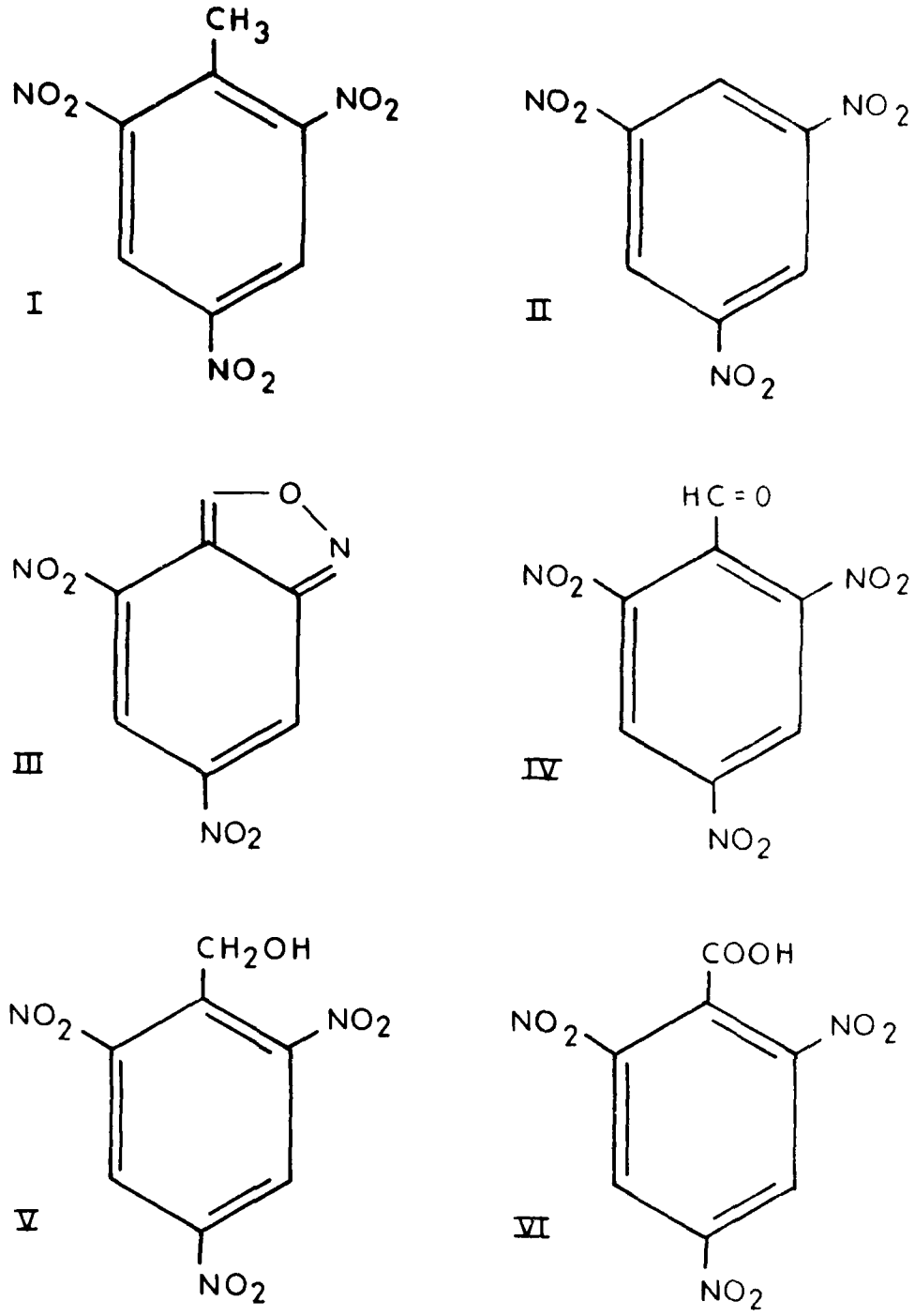

Figure 11. Compounds of importance in the thermal decomposition of TNT. (I) trinitrotoluene; (II) trinitrobenzene; (III) 4,6-dinitroanthranil; (IV) 2,4,6-trinitrobenzaldehyde; (V) 2,4,6-trinitrobenzyl alcohol; (VI) 2,4,6-trinitrobenzoic acid.

TABLE 6. PRODUCT DISTRIBUTION FROM THERMAL DECOMPOSITION OF TNT MAINTAINED 16 HOURS AT 200°C

Compound	Weight Per Cent
unreacted TNT	75-90
4,6-dinitroanthranil	2-4
2,4,6-trinitrobenzaldehyde	1-2
2,4,6-trinitrobenzyl alcohol	0.1-0.2
compound a, m.p. 217-8	∿ 0.1
compound b, m.p. 225-7	0.1-0.2
compound c, m.p. 132-4	∿ 0.04
compound d, m.p. 221-2	∿ 0.1
explosive coke	0-13

Product distribution from thermal decomposition of TNT maintained 16 hrs at 200°C, from Ref. 27. Compounds a-d are unidentified except for their melting points, which are listed in °C.

Raman spectrum of TNT itself, and more recent papers concerning the Raman[34] and infrared[35] spectra of trinitrobenzene (TNB). For the TNT in particular, its SRS spectrum should be obtainable with relative ease and considerably better quality than in the 1948 work[33].

Many of the strong peaks observed in TNB are attributable to modes involving the NO_2 group[34,35], and may well be present for nearly all of the trinitro compounds sought. If there are not significant shifts in these frequencies, little selectivity would be obtained. A comparison can be made between TNB and methyl 2,4,6-trinitrobenzoate[36] (the methyl ester of the acid VI of Fig 11)[34]. Of the six strong bands assigned to C-N or NO_2 in TNB, only two are observed in the ester, and they are displaced a few cm^{-1} from the TNB positions. If these modes can be used for analysis, a careful assignment using known compounds must be made.

On the other hand, the methyl 2,4,6-trinitrobenzoate exhibits a Raman line at 1605 cm^{-1}, similar to that of other trinitro esters[36]. This is also in the same position as that of (unnitrated) benzoic acid[17]. Nitration in TNB does not much affect ring modes (benzene: 992 cm^{-1}; TNB 1002) or CH (benzene: 3063; TNB: 3100). This evidence suggests that a useful guide might be provided by the Raman spectra of the unnitrated compounds. Strong and promising bands for this purpose, taken from an examination of the laser Raman spectra in Ref. 17 and a pre-laser paper[37] for anthranil, are listed in Table 7. All of the compounds have ring vibrations near 1000 cm^{-1} and CH stretches near 3100, so these bands will exhibit little selectivity. Benzene itself may be the most problematic for locating a non-interfering band. The double-peaked and broad band at 814 cm^{-1} of benzyl alcohol, the most promising region for this species,

---

[34] *H. F. Shurvell, A. R. Norris and D. E. Irish, "Raman and Far Infrared Spectra of S-trinitrobenzene and S-trinitrobenzene-d_3", Can. J. Chem. 47, 3515-3519 (1969).*

[35] *V. A. Osipov, V. A. Shylapochnikov and E. F. Ponizovtsev, "Vibrational Spectra of Aromatic Nitro Compounds", Zhur. Prik. Spekt. 8, 1003-1005 (1968).*

[36] *E. I. Kaminskaya, S. S. Gitis, and A. Ya. Kaminskii, "Raman Spectra of the σ-complexes between Aromatic Polynitro Compounds and Alcoholates", Zhur. Prik. Spekt. 26, 1053-1058 (1977).*

[37] *K. W. F. Kohlrausch and R. Seka, "Raman-Effekt und Konstitutions-Probleme, XIII. Mitteil.: Napthalinartig Kondensierte Hetero-biegelen", Ber. 71B, 1563-1570 (1938).*

TABLE 7. RAMAN FREQUENCIES OF UNNITRATED ANALOGS OF COMPOUNDS IN FIGURE 11

SPECIES	FREQUENCY (cm^{-1})
benzene	606
	1176
toluene	522
	788
	1380
benzyl alcohol	814
benzaldehyde	1701
benzoic acid	1292
	1605
anthranil	1450
	1500

Raman frequencies of unnitrated analogs of compounds in Figure 11. The bands most likely free of interference from other compounds in the table are listed.

may suffer from interference due to benzaldehyde at 828, benzoic acid at 788 or toluene at 798 cm^{-1}. For the other molecules listed, the peaks given should be relatively free of interferences.

Of course, to cover all of these bands, more than one dye will be necessary. The mixture of rhodamine 6G and rhodamine 640 would be useful for this. Bands closer than 500-600 cm^{-1} are not considered since filtering out the strong ruby pumping line, prior to dispersion within the monochromator, becomes exceedingly difficult for these small shifts.

C. Narrow-band probe IRS

As noted in the preceding section, little is known concerning the Raman spectra of the nitrated species of known or potential importance in TNT thermal decomposition. It would be valuable to independently obtain such spectra on known samples, in order to facilitate assignments in this and other work. To assess potential problems with interferences and overlaps, it would be additionally useful to run spectra on mixtures of these compounds and/or their (less expensive) non-nitrated analogs.

These spectra should be obtained first using SRS in the now-standard and conventional configuration (AR+ laser, double monochromator, photon counting) so as to provide a rapid catalogue of each species Raman spectrum, and the spectrum of various mixtures.

Following this, IRS data on static mixtures should be obtained using a narrow-band, tunable probe laser. Here, the ruby laser would again provide the pump beam at ω, but the beam at ω_2 would be a continuous-duty dye laser pumped by an Ar^+ or Kr^+ laser. Tuning the dye laser provides the inverse Raman spectrum with no need for dispersion through a monochromator. Consequently a fast diode detector can be used. Its output would then be measured using a narrow gate boxcar integrator, so that only the dye radiation (at the tuned wavelength) during the ruby pulse would be detected. Standard differencing techniques, using a second boxcar gate sampling after the ruby pulse, would directly provide the inverse Raman absorption spectrum.

The utility of this narrow band method lies in its better signal to noise ratio (compared with single-shot, broadband IRS), which in turn is due to the stability of continuous duty dye lasers and the ability to average over several ruby pulses. The information obtained here would be the relative intensities of the bands whose positions were earlier located using SRS.

In particular, the use of the narrow band tunable dye would ensure that the observed linewidths were the actual Raman linewidths discussed in Section III D2. This method is perhaps the best way to measure these necessary but generally unavailable linewidth quantities so as to obtain integrated inverse Raman absorption coefficients. Such an experiment has been carried out on the 3062 and 3048 cm^{-1} bands of benzene; a

brief discussion and a figure are contained in an overall review[38] of the East German work in IRS.

D. Broadband CARS

It has already been mentioned (Section II B3) that broadband CARS, which has been used to date in gases[11] but not in liquids, is a promising competitive technique to IRS for the applications envisaged here.

For both techniques, the sensitivity would appear to be limited to detection of mole fractions of the order of 0.01 in a 1 cm cell, although this is due to different causes. In IRS, the limit is set by the smallest degree of measureable absorption. In CARS, the limit is set by the noise in the non-resonant background. An important difference, however, is in the path length dependence. In IRS, the absorption depends exponentially on path length, so the minimum detection limit will be higher for a shorter cell. For CARS, the sensitivity limit depends on the ratio of resonant to non-resonant signals which is path length independent.

In addition, CARS signals can be generated only over a path where the three beams retain the necessary phase-matching condition. In liquids, this "coherence length" is typically of the order of 1 mm[39]. Thus CARS may be especially suitable for measurements on processes (such as detonations) in which a short path length is desirable.

Using the notation developed earlier, we rewrite Eqs (59) and (60) of Eckbreth et al[4] for the power P_3 produced in a CARS beam at frequency ω_3:

$$P_3 = \frac{N^2 \, (d\sigma/d\Omega)^2 \, (I_1^2/h^2)\omega_3^2 \, z^2 \, P_2 \, \eta^4}{\pi^4 \, C^4 \, \omega_2 \, \Delta\omega} \quad . \qquad (19)$$

Here I_1 is the intensity (erg cm^{-2} sec^{-1}) of the pump beam, P_2 is the power in the probe at frequency ω_2 and z is the path length (the coherence length forms an upper bound on z). All frequencies and the Raman linewidth are in cm^{-1} in Eq (19). This expression ignores* population of

---

[38] A. Lau, W. Werncke, M. Pfeiffer, K. Lenz and H. Weigmann, "Inverse Raman Scattering", Sov. Journ. Quant. Elec. 3, 402-409 (1976).

[39] F. F. Begley, A. B. Harvey and R. L. Byer, "Coherent Anti-Stokes Raman Spectroscopy", Appl. Phys. Lett. 25, 387-390 (1974).

*Eckbreth et al.,[4] include it in their equations; we have dropped it.

the upper vibrational level either by thermal or laser-stimulated means.

The conversion efficiency P_3/P_2 has been calculated for the lasers considered in Section III E. This computation used the parameters for benzene discussed earlier (Section III D) and the coherence length value of 1 mm for z. The results are collected in Table 8. The extremely high conversion efficiencies for the Nd:YAG and DL14 systems are unrealistic in that laser pumping of the excited level should be taken into account, but clearly they promise extremely strong signals. To put in perspective the lower conversion efficiencies consider a 1 mJ/pulse* stokes beam at ω_2. This will produce about 5×10^{-8} J of CARS signal, or over 10^{11} antistokes photons, which is more than ample for detection. For a broadband signal, this when dispersed over the 500 channels of an OMA will still provide considerable signal.

Thus CARS signals can be generated over short path lengths, and at pump laser intensities considerably lower than 10^9 watt/cm^2. This is quite encouraging for use on detonating condensed phases, where it is desired to keep path lengths short but still avoid the problem of window damage discussed in Section III F.

A ruby laser was not considered in these calculations. Obviously there would be ample signal strength, and a ruby laser has been used in the pioneering broadband CARS experiments on gases[11]. While extensive and impressive results[40] have been obtained with such a system, the problems[40] in working with the necessary infrared dyes render the choice of a ruby much less attractive.

We again note that it is possible that the variation in phase match angle with wavelength, due to changes of the index of refraction of the liquid phase, may hamper broadband CARS in liquids. However the available evidence using a tuned probe laser[12,13] encourages optimism on this point.

There are two potential serious disadvantages with CARS, compared to IRS, for the desired application. The first is difficulty of alignment in a complex experimental environment such as that for a detonation experiment. The second is the problem of extracting quantitative information concerning species, especially in a mixture, due to the complex nature of a CARS spectrum.

We first consider the alignment problem. For CARS in a liquid, it is necessary to cross the beams at the focus and at a specific angle in order to generate the desired signals. For an experiment in which species

---

This 1 mJ must be the energy provided by the probe laser over the pulse duration of the pump laser.

[10] *W. B. Roh, "Coherent Anti-Stokes Raman Scattering of Molecular Gases", Air Force Aero Propulsion Laboratory, August 1977, AFAPL-TR-77-47.*

TABLE 8. CONVERSION EFFICIENCIES FOR SOME COMMERCIALLY AVAILABLE LASERS

laser	power at focus, Watt/cm^2	λ, nm	P_3/P_2 [Eq(19)]
Nd:YAG	1.6×10^9	532	0.21
CMX4	1.9×10^7	590	6.3×10^{-5}
NRG	1.4×10^7	590	3.4×10^{-5}
DL14	7.6×10^8	590	0.10

concentrations change, the resulting change in refractive index may render this difficult. This is not anticipated to be a problem with IRS since the beams may be made collinear. In addition, simply attaining the proper beam alignment may prove more difficult with CARS, particularly in a more hostile environment associated with remote probing of a detonating system. It has been our experience that the alignment of the beams in our IRS experiments is not always trivial and it is our expectation that CARS will be less forgiving than IRS in this connection. Ease of carrying out the experiment should not be neglected in making the comparison.

The alignment problem can presumably be overcome through careful and experienced technique. The second problem, however, is inherent in the CARS process itself. The CARS signals are composed of peaks, due to the resonant part of the third order susceptibility $\chi^{(3)}$, as expressed in Eq (10), and a slowly varying non-resonant part. Since the signal intensity at a frequency ω is proportional to $|\chi^{(3)}(\omega)|^2$, these two portions can interfere. One may express[18] the overall $\chi(3)$ in terms of the real (χ') and imaginary (χ'') parts of the resonant susceptibility and an added non-resonant term χ^{NR}, which is real:

$$\chi^{(3)} = \chi' + i\chi'' + \chi^{NR}, \tag{20}$$

The CARS signal intensity is then proportional to

$$|\chi^{(3)}|^2 = (\chi' + \chi^{NR})^2 + (\chi'')^2$$

$$(\chi')^2 + 2\chi'\chi^{NR} + (\chi^{NR})^2 + (\chi'')^2 . \tag{21}$$

The mixing of the resonant and non-resonant parts, through the cross term $\chi'\chi^{NR}$ leads to an asymmetric shape, because (see Eq (10)) χ' has a dispersion lineshape while χ'' has a Lorentzian form. The shape and size of the signals observed is critically dependent on the relative sizes of the resonant and non-resonant contributions. This is well illustrated by theoretical curves for different ratios exhibited in Ref 18.

For a mixture of components having neighboring Raman peaks, the situation could become quite complex, and may well require calibration using known samples of similar composition of the same or similar* species. Probably the best way to extract quantitative information is to use computer simulation, as has been done for broadband CARS of nitrogen in

* *In the sense of their Raman spectrum.*

flames to extract the rotational temperature[41]. This requires independent knowledge of the Raman cross sections $d\sigma/d\Omega$ and linewidths $\Delta\omega$, which could be obtained through the narrow-band IRS method discussed in Section VI C.

In conclusion, we find the results expressed in Table VIII quite encouraging for the use of broadband CARS as a diagnostic probe of a detonating condensed phase system. The advantage of high signal levels at lower pump laser intensity and a shorter path length is offset by the possible complexity of the spectrum and the resulting difficulty in obtaining a quantitative analysis. It is not apparent to us which technique (CARS vs IRS) is preferably for the envisioned application, and the choice is likely best made on the basis of the system probed. In fact, a combination of the two techniques may be the optimum. This could be provided by a Nd:YAG laser frequency doubled to 532 nm as the pump beam. The 532 nm would also pump the broadband dye used as the CARS Stokes laser at ω_2; the frequency tripled output of the Nd:YAG would pump the IRS probe laser at ω_2. Alternatively, the 532 nm beam could pump two dye lasers, one of which* would be the ω_1 pump and the other of which would be the ω_2 probe. Even were CARS to prove a superior technique for the actual diagnostic work, the narrow-band IRS experiments would be the better way to obtain the needed absorption coefficients and linewidths. This would be readily accomplished using the same frequency-doubled Nd:YAG as the pump and a ion-laser-pumped** continuous duty laser as the probe.

E. Recommendations

In particular for the BRL, we recommend that the future direction of this project be as follows. (1) Acquire a Nd:YAG laser and associated dye laser. (2) Establish and develop broadband CARS. Initial experiments here for evaluation purposes could be done with the CMX4 and/or NRG lasers on hand, but with the objective of later conversion to Nd:YAG operation. (3) Establish and develop narrow-band tunable IRS for the determination of Raman cross sections and linewidths. The ruby laser would be used for at least initial experiments. (4) Carry out measurements on the non-nitrated analogs of the compounds in Figure 11, individually and in mixtures, using, in sequence SRS, narrow-band IRS, broadband IRS and (if then available) broadband CARS. (5) Carry out the same sequence of measurements for trinitrobenzene, trinitrotoluene, and as many of the

---

[41] *A. C. Eckbreth and R. J. Hall, "CARS Diagnostic Investigations of Flames", Proceedings of Tenth Materials Research Symposium on Characterization of High Temperature Vapors and Gases, Gaithersburg, Maryland, September 1978.*

* *The laser at shorter wavelength for CARS, and the one at longer wavelength for IRS.*

** *Here one would likely need to pump using the ultraviolet lines of Ar+ or Kr+, so as to obtain dye output sufficiently blue of 532 nm.*

compounds in Figure 11 as it is economically feasible to synthesize. (6) Probe in situ the thermal decomposition of TNT using first infrared absorption and SRS, then IRS (narrow-and broadband) and broadband CARS. (7) In conjunction with appropriate personnel from Terminal Ballistics Division, give preliminary consideration to the design of a detonation experiment capable of being probed by lasers.

F. Addenda

Since the initial preparation of the material in this section, two papers have appeared which have bearing on the points discussed in Sections VI C and D.

Yeung and coworkers[42] have used a ruby pumping laser and continuous duty dye laser to carry out narrow-band inverse Raman measurements of the 1345 cm^{-1} line of nitrobenzene. Utilization of a dye laser narrower than the Raman linewidth permits an absolute cross section to be obtained from a measurement of the degree of absorption. Although a previously published value of the linewidth was used for the data analysis in Ref. 42 this quantity could presumably also be obtained by tuning of the dye laser and scanning the Raman line. A discussion of the problems associated with the pulse-to-pulse variation of the ruby laser (±20%) is included. A good case is made for the use of inverse Raman spectroscopy in this manner in order to determine cross sections, in accord with our conclusions in Section VIC and D.

Tretzel and Schneider[43] have carried out a broadband CARS measurement* on highly fluorescing acridine dyes, using two dye lasers pumped by a nitrogen laser and tuned so as to obtain resonant enhancement. A 1/3-m monochromator and OMA were used for detection. Quantitative intensity results are not given although it is clear that the refractive index variation does not preclude obtaining a CARS signal across the full range of the gain profile of the probe laser. In fact, a qualitative study of the spectrum as a function of crossing angle between 2.9° (the proper phase matching angle) and 0.7° was made. This exhibited considerable changes in the appearance of the spectrum due to the differing proportional contributions of the resonant and non-resonant parts of the susceptibility (Eqs (20) and (21)).

---

[42] *L. J. Hughes, L. E. Steenhoek and E. S. Yeung, "Determination of Absolute Raman Cross Section using the Inverse Raman Effect", Chem. Phys. Lett. 58, 413-416 (1978).*

[43] *J. Tretzel and F. W. Schneider, "Resonance Multiplex CARS of Fluorescing Acridines", Chem. Phys. Lett. 59, 514-518 (1978).*

* *Narrow-band probe lasers were also used for part of the experiments.*

While the work in Reference 43 demonstrates that CARS signals can be obtained without undue worry concerning the crossing angle problem across the full range of the probe dye, it especially underscores the inherent problems in obtaining quantitative results from the observed spectrum. In particular, careful attention must be paid to specification of the crossing angles when attempting an analysis of the data.

REFERENCES

1. W. VonHolle, "The Application of Inverse Raman Spectroscopy to Chemical Decomposition in Energetic Systems", BRL Memorandum Report No. 2607, March 1976. (AD #B010506L)

2. N. Bloembergen, Non-linear Optics, Benjamin, New York, 1965.

3. W. M. Tolles, G. L. Eesley and M. D. Levenson, "Heterodyne Detection of Coherent Signals", S.P.I.E. Conference, San Diego, Cal., August 1977.

4. A. C. Eckbreth, P. A. Bonczyk and J. F. Verdieck, "Laser Raman and Fluorescence Techniques for Practical Combustion Diagnostics", Appl. Spec. Rev. 12, 15-164 (1978).

5. A. C. Eckbreth, "BOXCARS: Crossed-Beam Phase-Matched CARS Generation in Gases", Appl. Phys. Lett., to be published.

6. S. H. Lin, E. S. Reid and C. J. Tredwell, "The Resonance Inverse Raman Effect", Chem. Phys. Lett. 29, 389-392 (1974).

7. W. Wernecke, J. Klein, A. Lau, K. Lenz, and G. Hunsalz, "Investigation of Inverse Raman Spectroscopy using the Method of Intracavity Spectroscopy", Opt. Comm. 11, 159-163 (1974).

8. G. L. Eesley, M. D. Levenson, and W. M. Tolles, "Optically Heterodyned Coherent Raman Spectroscopy", J. Quant. Elec., to be published.

9. W. VonHolle, private communication, May 1978.

10. D. Heiman, R. W. Hellwarth, M. D. Levenson and G. Martin, "Raman-Induced Kerr Effect", Phys. Rev. Lett. 36, 189-192 (1976).

11. W. B. Roh, P. W. Schreiber and J. P. E. Taran, "Single-pulse Coherent Anti-Stokes Raman Spectroscopy", Appl. Phys. Lett. 29, 174-176 (1976).

12. R. F. Begley, A. B. Harvey, R. L. Byer and B. S. Hudson, "Raman Spectroscopy with Intense, Coherent Anti-Stokes Beams", J. Chem. Phys. 61, 2466-2467 (1974).

13. A. B. Harvey, private communication, May 1978.

14. J. A. Koningstein, Introduction to the Theory of the Raman Effect, D. Reidel, Dordrecht, Holland, 1972, p. 142-144.

15. E. S. Yeung, "Inverse Raman Effect: A Quantitative Spectroscopic Technique", J. Mol. Spec. 53, 379-392 (1974).

16. J. B. Grun, A. K. McQuillan and B. P. Stoicheff, "Intensity and Gain Measurements on the Stimulated Emission in Liquid O_2 and N_2", Phys. Rev. 180, 61-68 (1969).

17. B. Schrader and W. Meier, ed., Raman/IR Atlas of Organic Compounds. Verlag Chemie, Weinheim, 1974.

18. W. M. Tolles, J. W. Nibler, J. R. McDonald, and A. B. Harvey, "A Review of the Theory and Application of Coherent Anti-Stokes Raman Spectroscopy (CARS)", Appl. Spect. 31, 253-271 (1977).

19. D. Steele, Theory of Vibrational Spectroscopy, Saunders, Philadelphia, 1971, p. 166ff.

20. G. Herzberg, Molecular Spectra and Molecular Structure. II. Infrared and Raman Spectra of Polyatomic Molecules, D. Van Nostrand, Princeton, 1945.

21. W. R. L. Clements and B. P. Stoicheff, "Raman Linewidths for Stimulated Threshold and Gain Calculations", Appl. Phys. Lett. 12, 246-248 (1968).

22. Handbook of Chemistry and Physics, Chemical Rubber Publishing Co., Cleveland (1955) and other editions.

23. A. DaMommio, in Fundamentals and Applications of Lasers. Volume I, Technical Education Research Center, Waco, Texas, 1976, p. 1-9-17ff.

24. J. W. Nibler, J. R. McDonald and A. B. Harvey, "CARS" Measurement of Vibrational Temperatures in Electric Discharges", Opt. Comm. 18, 371-373 (1976).

25. Symposium on Laser-Induced Chemistry, American Chemical Society Meeting, Anaheim, California, March 1978.

26. Y. Tsunoda, "Inverse Raman Effect of Some Organic Liquids", Jap. Journ. Appl. Phys. 11, 1293-1297 (1972).

27. F. C. Rauch and R. B. Wainright, "Studies on Composition B", Picatinny Arsenal, February 1969, AD-850 928.

28. R. N. Rogers, "Combined Pyrolysis and Thin Layer Chromatography, a Method for Study of Decomposition Mechanisms", Anal. Chem. 39, 730-733 (1967).

29. J. C. Dacons, M. J. Kamlet and D. V. Sickman, "Thermal Decomposition of TNT", NAVORD Report 6831, May 1960, AD-317 977.

30. F. C. Rauch and W. P. Colman, "Studies on Composition B", Picatinny Arsenal, March 1970, AD-869 226.

31. J. C. Dacons, H. G. Adolph and M. J. Kamlet, "Some Novel Observations Concerning the Thermal Decomposition of TNT", J. Phys. Chem. 74, 3035-3040 (1970); W. P. Colman and F. C. Rauch, "Studies on Composition B", Picatinny Arsenal, February 1971, AD-881 190.

32. S. A. Shackleford, J. W. Beckman and J. S. Wilkes, "Deuterium Isotope Effects in the Thermochemical Decomposition of Liquid 2,4,6-Trinitrotoluene: Application to Mechanistic Studies using Isothermal Differential Scanning Calorimetry Analysis", J. Org. Chem. 42, 4201-4206 (1977).

33. P. P. Shorygin, "Spectra of Combination Scattering and Special Features of the Structure of Organic Compounds", Zhur. Fiz. Khim. 22, 1409-1418 (1948).

34. H. F. Shurvell, A. R. Norris and D. E. Irish, "Raman and Far Infrared Specta of S-trinitrobenzene and S-trinitrobenzene-d_3", Can. J. Chem. 47, 2515-2519 (1969).

35. V. G. Osipov, V. A. Shylapochnikov and E. F. Ponizovtsev, "Vibrational Spectra of Aromatic Nitro Compounds", Zhur. Prik. Spekt. 8, 1003-1005 (1968).

36. E. G. Kaminskaya, S. S. Gitis, and A. Ya. Kaminskii, "Raman Spectra of the σ-complexes between Aromatic Polynitro Compounds and Alcoholates", Zhur. Prik. Spekt. 26, 1053-1058 (1977).

37 K. W. F. Kohlrausch and R. Seka, "Raman-Effekt und Konstitutions-Probleme, XIII. Mittelil.: Napthalinartig kondensierte Hetero-bicyclen", Ber. 71B, 1563-1570 (1938).

38. A. Lau, W. Werncke, M. Pfeiffer, K. Lenz and H. Weigmann, "Inverse Raman Scattering", Sov. Journ. Quant. Elec. 3, 402-409 (1976).

39. R. F. Begley, A. B. Harvey and R. L. Byer, "Coherent Anti-Stokes Raman Spectroscopy", Appl. Phys. Lett. 25, 387-390 (1974).

40. W. B. Roh, "Coherent Anti-Stokes Raman Scattering of Molecular Gases", Air Force Aero Propulsion Laboratory, August 1977, AFAPL-TR-77-47.

41. A. C. Eckbreth and R. J. Hall, "CARS Diagnostic Investigation of Flames", Proceedings of Tenth Materials Research Symposium on Characterization of High Temperature Vapors and Gases, Gaithersburg, Maryland, September 1978.

42. L. J. Hughes, L. E. Steenhoek and E. S. Yeung, "Determination of Absolute Raman Cross Section using the Inverse Raman Effects", Chem. Phys. Lett. 58, 413-416 (1978).

43. J. Tretzel and F. W. Schneider, "Resonance Multiplex CARS of Fluorescing Acridines", Chem. Phys. Lett. 59, 514-518 (1978).

DISTRIBUTION LIST

No. of Copies	Organization
12	Commander Defense Technical Info Center ATTN: DDC-DDA Cameron Station Alexandria, VA 22314
1	Director Defense Advanced Research Projects Agency ATTN: LTC C. Buck 1400 Wilson Boulevard Arlington, VA 22209
2	Director Institute for Defense Analyses ATTN: H. Wolfhard R.T. Oliver 400 Army-Navy Drive Arlington, VA 22202
1	Commander US Army Materiel Development and Readiness Command ATTN: DRCDMD-ST 5001 Eisenhower Avenue Alexandria, VA 22333
2	Commander US Army ARRADCOM ATTN: DRDAR-TSS Dover, NJ 07801
5	Commander US Army ARRADCOM ATTN: DRDAR-LCA, J. Lannon DRDAR-LC, J.P. Picard DRDAR-LCE, R.F. Walker DRDAR-SCA, L. Stiefel DRDAR-SC, L. Harris Dover, NJ 07801
1	Commander US Army ARRCOM ATTN: DRSAR-LEP-L, Tech Lib Rock Island, IL 61299
1	Director US Army ARRADCOM Benet Weapons Laboratory ATTN: DRDAR-LCB-TL Watervliet, NY 12189
1	Commander US Army Watervliet Arsenal ATTN: SARWV-RD, R. Thierry Watervliet, NY 12189
1	Commander US Army Aviation Research and Development Command ATTN: DRSAV-E 4300 Goodfellow Blvd St. Louis, MO 63120
1	Director US Army Air Mobility Research and Development Laboratory Ames Research Center Moffett Field, CA 94035
1	Commander US Army Communications Rsch and Development Command ATTN: DRDCO-PPA-SA Ft. Monmouth, NJ 07703
1	Commander US Army Electronics Rsch & Development Command Technical Support Activity ATTN: DELSD-L Ft. Monmouth, NJ 07703
1	Commander US Army Missile Command ATTN: DRSMI-R Redstone Arsenal, AL 35809
1	Commander US Army Missile Command ATTN: DRSMI-YDL Redstone Arsenal, AL 35809

DISTRIBUTION LIST

No. of Copies	Organization
1	Commander US Army Natick Research and Development Command ATTN: DRXRE, D. Sieling Natick, MA 01762
1	Commander US Army Tank Automotive Rsch and Development Command ATTN: DRDTA-UL Warren, MI 48090
1	Commander US Army White Sands Missile Range ATTN: STEWS-VT White Sands Missile Range, NM 88002
1	Commander US Army Materials & Mechanics Research Center ATTN: DRXMR-ATL Watertown, MA 02172
1	Commander US Army Research Office ATTN: Tech Lib Research Triangle Park, NC 27706
1	Director US Army TRADOC Systems Analysis Activity ATTN: ATAA-SL, Tech Lib White Sands Missiles Range, NM 88002
1	Office of Naval Research ATTN: Code 473 800 N. Quincy Street Arlington, VA 22217
1	Commander Naval Sea Systems Command ATTN: SEA-62R2, J.W. Murrin National Center Bldg. 2, Room 6E08 Washington, DC 20362
1	Commander Naval Surface Weapons Center ATTN: Library Br, DX-21 Dahlgren, VA 22448
2	Commander Naval Surface Weapons Center ATTN: Code 240, S.J. Jacobs Code 730 Silver Spring, MD 20910
1	Commander Naval Underwater Systems Center Energy Conversion Department ATTN: Code 5B331, R.S. Lasar Newport, RI 02840
2	Commander US Naval Weapons Center ATTN: R. Derr C. Thelen China Lake, CA 93555
3	Commander Naval Research Laboratory ATTN: Code 6180 A.B. Harvey J.R. McDonald Washington, DC 20375
4	Superintendent Naval Postgraduate School ATTN: Tech Lib D. Netzer A. Fuhs W. Tolles Monterey, CA 93940

DISTRIBUTION LIST

No. of Copies	Organization
2	Commander Naval Ordnance Station ATTN: S. Mitchell Tech Lib Indian Head, MD 20640
2	AFOSR ATTN: L. Caveny B.T. Wolfson Bolling AFB, DC 20332
3	AFRPL (DYSC) ATTN: D. George J.N. Levine B. Goshgarian Edwards AFB, CA 93523
2	AFAPL ATTN: P.W. Schreiber M. Roquemore Wright-Patterson AFB, OH 45433
1	National Bureau of Standards ATTN: T. Kashiwagi Washington, DC 20234
2	Lawrence Livermore Laboratory ATTN: W.G. VonHolle R.A. McWilliams Livermore, CA 94550
1	Lockheed Palo Alto Rsch Labs ATTN: Tech Info Ctr 3521 Hanover Street Palo Alto, CA 94304
1	Aerojet Solid Propulsion Co. ATTN: P. Micheli Sacramento, CA 95813
1	ARO Incorporated ATTN: N. Dougherty Arnold AFS, TN 37389
1	Atlantic Research Corporation ATTN: M.K. King 5390 Cherokee Avenue Alexandria, VA 22314
1	AVCO Corporation AVCO Everett Research Lab Div ATTN: D. Stickler 2385 Revere Beach Parkway Everett, MA 02149
1	Calspan Corporation ATTN: E.B. Fisher P.O. Box 400 Buffalo, NY 14211
1	Foster Miller Associates, Inc. ATTN: A.J. Erickson 135 Second Avenue Waltham, MA 02154
1	General Electric Company Armament Department ATTN: M.J. Bulman Lakeside Avenue Burlington, VT 05402
1	General Electric Company Flight Propulsion Division ATTN: Tech Lib Cincinnati, OH 45215
2	General Motors Research Lab ATTN: T.D. Fansler G. Eesley Warren, MI 48090
1	Geo-Centers, Inc. ATTN: M.E. McIlwain 381 Elliot Street Newton Upper Falls, MA 02164
2	Hercules Incorporated Alleghany Ballistics Lab ATTN: R. Miller Tech Lib Cumberland, MD 21501

DISTRIBUTION LIST

No. of Copies	Organization
1	IITRI ATTN: M.J. Klein 10 West 35th Street Chicago, IL 60615
1	Olin Corporation Badger Army Ammunition Plant ATTN: J. Rammarace Baraboo, WI 53913
2	Olin Corporation New Haven Plant ATTN: R.L. Cook D.W. Riefler 275 Winchester Avenue New Haven, CT 06504
1	Paul Gough Associates, Inc. ATTN: P.S. Gough P.O. Box 1614 Portsmouth, NH 03801
1	Physics International Company 2700 Merced Street Leandro, CA 94577
1	Pulsepower Systems, Inc. ATTN: L.C. Elmore 815 American Street San Carlos, CA 94070
3	Rockwell International Corp. Rocketdyne Division ATTN: C. Obert J.E. Flanagan A. Axeworthy 6633 Canoga Avenue Canoga Park, CA 91304
2	Rockwell International Corp. Rocketdyne Division ATTN: W. Haymes Tech Lib McGregor, TX 76657
3	Sandia Laboratories ATTN: D.L. Hartley P. Mattern L.A. Rahn Livermore, CA 94550
1	Sandia Laboratories ATTN: A. Owyoung Albuquerque, NM 87115
1	Science Applications, Inc. ATTN: R.B. Edelman 23146 Cumorah Crest Woodland Hills, CA 91364
1	Shock Hydrodynamics, Inc. ATTN: W.H. Anderson 4710-16 Vineland Avenue North Hollywood, CA 91602
1	Thiokol Corporation Elkton Division ATTN: E. Sutton Elkton, MD 21921
3	Thiokol Corporation Huntsville Division ATTN: D. Flanigan R. Glick Tech Lib Huntsville, AL 35807
2	Thiokol Corporation Wasatch Division ATTN: J. Peterson Tech Lib P.O. Box 524 Brigham City, UT 84302
1	TRW Systems Group ATTN: H. Korman One Space Park Redondo Beach, CA 90278

DISTRIBUTION LIST

No. of Copies	Organization
1	United Technologies Rsch Ctr ATTN: A. Eckbreth East Hartford, CT 06108
2	United Technologies ATTN: R. Brown Tech Lib P.O. Box 358 Sunnyvale, CA 94086
1	Universal Propulsion Co. ATTN: H.J. McSpadden 1800 W. Deer Valley Road Phoenix, AZ 85027
1	Battelle Memorial Institute ATTN: Tech Lib 505 King Avenue Columbus, OH 43201
1	Brigham Young University Dept. of Chemical Engineering ATTN: M.W. Beckstead Provo, UT 84601
1	California Institute of Tech. 204 Karmar Lab ATTN: F.E.C. Culick 1201 E. California Street Pasadena, CA 91125
1	Case Western Reserve Univ. Division of Aerospace Sciences ATTN: J. Tien Cleveland, OH 44135
3	Georgia Institute of Tech. School of Aerospace Engineering ATTN: B.T. Zinn E. Price W.C. Strahle Atlanta, GA 30332
1	Institute of Gas Technology ATTN: D. Gidaspow 3424 S. State Street Chicago, IL 60616
1	Iowa State University Dept. of Chemistry ATTN: E.S. Yeung Ames, IA 50011
1	Johns Hopkins University/APL Chemical Propulsion Info Agency ATTN: T. Christian Johns Hopkins Road Laurel, MD 20810
1	Massachusetts Institute of Technology Dept. of Mechanical Engineering ATTN: T. Toong Cambridge, MD 02139
1	Oregon State University Dept. of Chemistry ATTN: J.W. Nibler Corvallis, OR 97330
1	Pennsylvania State University Applied Research Laboratory ATTN: G.M. Faeth P.O. Box 30 State College, PA 16801
1	Pennsylvania State University Dept. of Mechanical Engineering ATTN: K. Kuo University Park, PA 16801
1	Pennsylvania State University Dept. of Material Sciences ATTN: H. Palmer University Park, PA 16810

DISTRIBUTION LIST

No. of Copies	Organization
1	Princeton University Forrestal Campus ATTN: Tech Lib P.O. Box 710 Princeton, NJ 08540
1	Purdue University School of Mechanical Engineering ATTN: J. Osborn TSPC Chaffee Hall West Lafayette, IN 47906
1	Purdue University Dept. of Chemistry ATTN: F.E. Lytle West Lafayette, IN 47906
1	Rutgers State University Dept. of Mechanical and Aerospace Engineering ATTN: S. Temkin University Heights Campus New Brunswick, NJ 08903
14	SRI International ATTN: Tech Lib D. Crosley (10 copies) J. Barker D. Golden D. McMillen 333 Ravenswood Avenue Menlo Park, CA 94025
1	Stevens Institute of Tech. Davidson Laboratory ATTN: R. McAlevy, III Hoboken, NJ 07030
1	University of Illinois Dept. of Aeronautical Engineering ATTN: H. Krier Transporation Bldg., Rm 105 Urbana, IL 61801
1	University of Minnesota Dept. of Mechanical Engineering ATTN: E. Fletcher Minneapolis, MN 55455
2	University of Southern California Dept. of Chemistry ATTN: S. Benson O. Schnepp Los Angeles, CA 90007
2	University of Texas Dept. of Chemistry ATTN: W. Gardiner H. Schaefer Austin, TX 78712
2	University of Utah Dept. of Chemical Engineering ATTN: A. Baer G. Flandro Salt Lake City, UT 84112

Aberdeen Proving Ground

Dir, USAMSAA
ATTN: DRXSY-D
DRXSY-MP, H. Cohen

Cdr, USATECOM
ATTN: DRSTE-TO-F

Dir, USACSL, Bldg. E3516, EA
ATTN: DRDAR-CLB-PA

USER EVALUATION OF REPORT

Please take a few minutes to answer the questions below; tear out this sheet, fold as indicated, staple or tape closed, and place in the mail. Your comments will provide us with information for improving future reports.

1. BRL Report Number _____

2. Does this report satisfy a need? (Comment on purpose, related project, or other area of interest for which report will be used.)

_____

_____

_____

3. How, specifically, is the report being used? (Information source, design data or procedure, management procedure, source of ideas, etc.) _____

_____

_____

4. Has the information in this report led to any quantitative savings as far as man-hours/contract dollars saved, operating costs avoided, efficiencies achieved, etc.? If so, please elaborate.

_____

_____

5. General Comments (Indicate what you think should be changed to make this report and future reports of this type more responsive to your needs, more usable, improve readability, etc.) _____

_____

_____

_____

6. If you would like to be contacted by the personnel who prepared this report to raise specific questions or discuss the topic, please fill in the following information.

Name: _____

Telephone Number: _____

Organization Address: _____

_____

_____

FOLD HERE

Director
US Army Ballistic Research Laboratory
Aberdeen Proving Ground, MD 21005

NO POSTAGE
NECESSARY
IF MAILED
IN THE
UNITED STATES

OFFICIAL BUSINESS
PENALTY FOR PRIVATE USE, $300

BUSINESS REPLY MAIL
FIRST CLASS PERMIT NO 12062 WASHINGTON, DC
POSTAGE WILL BE PAID BY DEPARTMENT OF THE ARMY

Director
US Army Ballistic Research Laboratory
ATTN: DRDAR-TSB
Aberdeen Proving Ground, MD 21005

FOLD HERE